JOURNAL OF GEOPHYSICAL RESEARCH, VOL. 102, NO. B7, PAGES 15,463–15,487, JULY 10, 1997

The Southeast Indian Ridge between 88°E and 118°E: Gravity anomalies and crustal accretion at intermediate spreading rates

James R. Cochran

Lamont-Doherty Earth Observatory Columbia University, Palisades, New York

Jean-Christophe Sempéré [1,2]

School of Oceanography, University of Washington, Seattle

SEIR Scientific Team [3]

Abstract. Although slow spreading ridges characterized by a deep axial valley and fast spreading ridges characterized by an axial bathymetric high have been extensively studied, the transition between these two modes of axial morphology is not well understood. We conducted a geophysical survey of the intermediate spreading rate Southeast Indian Ridge between 88°E and 118°E, a 2300-km-long section of the ridge located between the Amsterdam hot spot and the Australian-Antarctic Discordance where satellite gravity data suggest that the Southeast Indian Ridge (SEIR) undergoes a change from an axial high in the west to an axial valley in the east. A basic change in axial morphology is found near 103°30'E in the shipboard data; the axis to the west is marked by an axial high, while a valley is found to the east. Although a well-developed axial high, characteristic of the East Pacific Rise (EPR), is occasionally present, the more common observation is a rifted high that is lower and pervasively faulted, sometimes with significant (> 50 m throw) faults within a kilometer of the axis. A shallow axial valley (< 700 m deep) is observed from 104°E to 114°E with a sudden change to a deep (>1200 m deep) valley across a transform at 114°E. The changes in axial morphology along the SEIR are accompanied by a 500 m increase in near-axis ridge flank depth from 2800 m near 88°E to 3300 m near 114°E and by a 50 mGal increase in the regional level of mantle Bouguer gravity anomalies over the same distance. The regional changes in depth and mantle Bouguer anomaly (MBA) gravity can be both explained by a 1.7-2.4 km change in crustal thickness or by a mantle temperature change of 50°C-90°C. In reality, melt supply (crustal thickness) and mantle temperature are linked, so that changes in both may occur simultaneously and these estimates serve as upper bounds. The along-axis MBA gradient is not uniform. Pronounced steps in the regional level of the MBA gravity occur at 103°30'E-104°E and at 114°E-116°E and correspond to the changes in the nature of the axial morphology and in the amplitude of abyssal hill morphology suggesting that the different forms of morphology do not grade into each other but rather represent distinctly different forms of axial structure and tectonics with a sharp transition between them. The change from an axial high to an axial valley requires a threshold effect in which the strength of the lithosphere changes quickly. The presence or absence of a quasi-steady state magma chamber may provide such a mechanism. The different forms of axial morphology are also associated with different intrasegment MBA gravity patterns. Segments with an axial high have an MBA low located at a depth minimum near the center of the segment. At EPR-like segments, the MBA low is about 10 mGal with along-axis gradients of 0.15-0.25 mGal/km, similar to those observed at the EPR. Rifted highs have a shallower low and lower gradients suggesting an attenuated composite magma chamber and a reduced and perhaps episodic melt supply. Segments with a shallow axial valley have very flat along-axis MBA profiles with little correspondence between axial depth and axial MBA gravity.

Introduction

The morphology of fast spreading and slow spreading mid-ocean ridges differs dramatically. Fast spreading ridges, such as the East Pacific Rise spreading at 65-150 mm/yr, are characterized by an approximately 20-km-wide, 200- to 400-m-high ridge axis high and relatively low relief (50-150 m) abyssal hills on the ridge flanks [*Menard*, 1960; *Macdonald*, 1989]

Paper number 97JB00511.
0148-0227/97/97JB-00511$09.00

[1]Also at Groupe de Recherche en Géodésie Spatiale, UMR-5566, Observatorie Midi-Pyrénées, Toulouse, France.

[2]Now at Exxon Production Research Company, Houston, Texas.

[3]Southeast Indian Ridge (SEIR) Scientific Team (D. Christie, College of Oceanic and Atmospheric Sciences, Oregon State University; M. Eberle, Department of Geological Science, Brown University; L. Gelí, Départment de Géosciences Marines, IFREMER; J. A. Goff, University of Texas Institute of Geophysics,; H. Kimura, Earthquake Research Institute, University of Tokyo; Y. Ma, Lamont-Doherty Earth Observatory of Columbia University; A. Shah, School of Oceanography, University of Washington; C. Small, Lamont-Doherty Earth Observatory of Columbia University; B. Sylvander, College of Oceanic and Atmospheric Sciences, Oregon State University; B. P. West, School of Oceanography, University of Washington; and W. Zhang, Lamont-Doherty Earth Observatory of Columbia University).

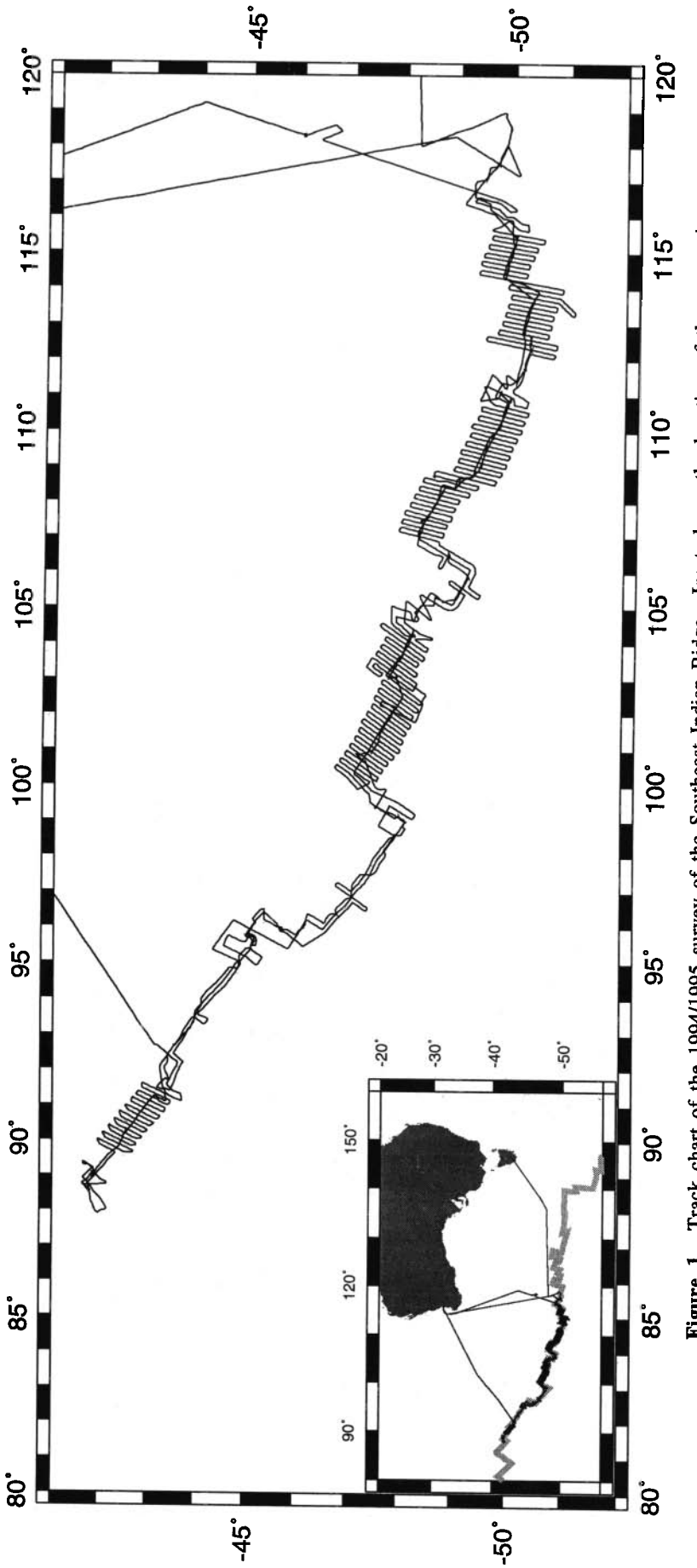

Figure 1. Track chart of the 1994/1995 survey of the Southeast Indian Ridge. Inset shows the location of the survey in relation to Australia and the Australian-Antarctic plate boundary.

Slow spreading ridges, such as the Mid-Atlantic Ridge spreading at 20-40 mm/yr, are associated with 1- to 2-km deep, 25- to 40-km-wide axial rift valleys and much rougher (> 500 m relief) abyssal hills on the ridge flanks [*Heezen*, 1960; *Macdonald*, 1986].

Although the basic difference in the morphology of "Atlantic-type" and "Pacific-type" ridges has been known for over 35 years, it is still not completely understood. How the same basic processes of plate separation, mantle upwelling, and decompression melting result in such fundamentally different morphology and tectonics is a basic question in understanding crustal accretion. Intermediate spreading rate ridges can provide information on crustal accretion in conditions other than those represented by the well-studied end-members and in particular allow the nature of the transition between the very different slow spreading and fast spreading end-member axial structures to be examined. The nature of the transition is an important observation in constraining models for the creation of axial morphology [e.g., *Chen and Morgan*, 1990; *Phipps Morgan et al.*, 1987]. However, in spite of their potential importance in understanding crustal accretion and the processes that create seafloor morphology, intermediate spreading rate ridges have not been studied nearly as intensely as have fast and slow spreading ridges.

Field Program

During the Austral summer of 1994/1995, a geophysical survey of the intermediate spreading rate Southeast Indian Ridge (SEIR) from 88°E to 118°E was carried out on two legs of the "Westward" expedition on R/V *Melville* (Figure 1). The objectives of the field program were (1) to investigate changes in axial morphology accompanying the west to east increase in ridge axis depth, including in particular the transition from axial high to axial valley observed near 101°E [*Small and Sandwell*, 1992; *Ma and Cochran*, 1996], (2) to investigate possible changes in melt supply and distribution within segments (as evidenced by gravity anomalies) accompanying the change in axial morphology and (3) to determine geochemical variations along the ridge which were hypothesized to accompany the transition in morphology.

The first leg of the field program conducted a geophysical survey of the ridge axis and flanks between 91°E and 118°E. The second leg was primarily devoted to rock sampling but also obtained additional geophysical coverage between 88°E

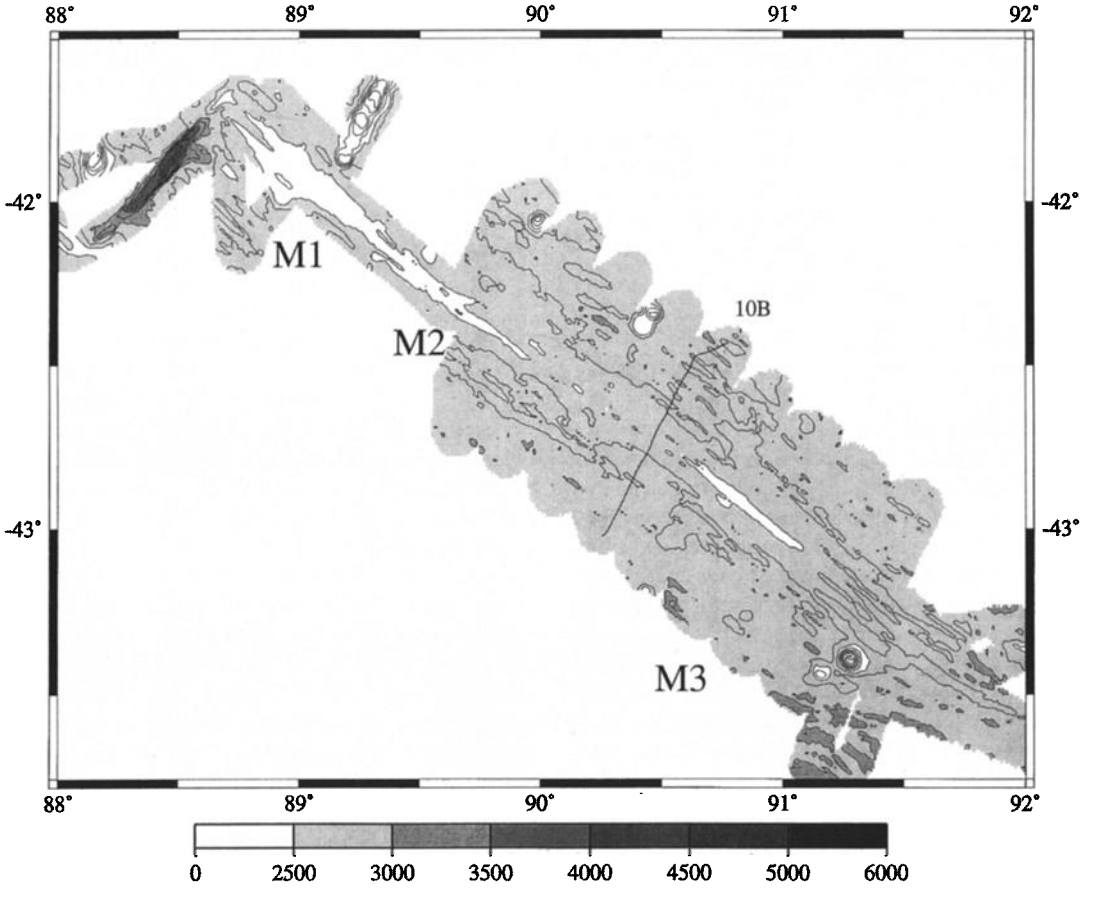

Figure 2. Bathymetric map of detailed survey box 0 at the very western end of the survey area (Figure 1). The bathymetry is contoured at 250-m intervals and color changes occur at 500-m intervals. The detailed survey extends out to approximately 1.2 Ma seafloor on both flanks. Solid line shows the location of center beam bathymetry and free-air gravity profile shown in Figure 10 (10B). This map includes second-order segments M1, M2, and M3 (Figures 7 and 8) which are the shallowest in the survey area (Figure 7). The next two segments to the west (K and L) are the shallowest on the SEIR [*Johnson et al.*, 1996; *Ma and Cochran*, 1996]. The central portions of segments M1 and M2 have EPR-like axial highs, but a rifted axial high characterizes most of the survey box.

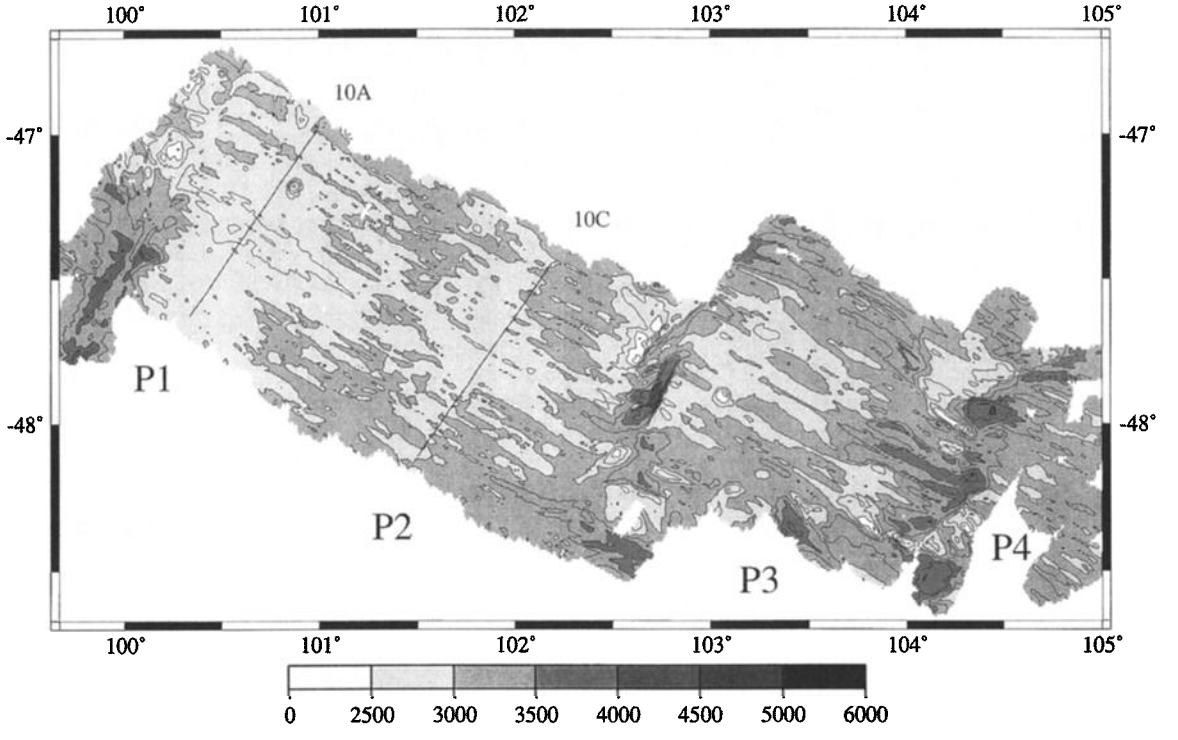

Figure 3. Bathymetric map of detailed survey box 1. The bathymetry is contoured at 250-m intervals, and shading changes occur at 500-m intervals. The detailed survey extends out to approximately 1.2 Ma seafloor on both flanks. Solid lines show the location of center beam bathymetry and free-air gravity profiles shown in Figure 10 (10A and 10C). This map includes second-order segments P1, P2, P3, and P4 (Figures 7 and 8). The central portion of segment P1, immediately to the east of the left-stepping 100°E transform, has an EPR-like axial high. Segment P2 is characterized by a rifted high and is typical of the majority of segments west of 103°E. Segment S4 marks the western end of a region extending eastward to 129°E in which the SEIR is characterized by an axial valley. Note that the transform at 102°45'E has evolved from a nontransform offset since 1 Ma.

and 91°E. A 2300-km-long segment of the ridge axis was surveyed during the two legs including four detailed study "boxes" which extend for a total of 1100 km along the axis (Figure 1) and include eight second-order ridge segments. Within each box, Seabeam 2000 bathymetry, gravity, and magnetics lines perpendicular or slightly oblique to the ridge axis extending roughly 45 km (1.2 Myr) away from the axis on each flank were obtained at 9-km intervals. This spacing provides essentially complete bathymetric coverage and gravity and magnetics lines at close enough spacing to allow confident interpolation between tracks. Bathymetric maps of the four survey boxes are shown in Figures 2-5.

This is one of two papers presenting preliminary geophysical results from the two cruises. The companion paper by *Sempere et al.* [this issue] discusses the segmentation, axial depth, and long-wavelength temperature variations along the SEIR. In this paper, we will concentrate on the pattern of gravity anomalies, their relationship to axial morphology and what they reveal about crustal accretion at intermediate spreading rates.

Gravity Data Collection and Reduction

Gravity data were collected throughout the survey of the SEIR using a Bell Aerospace BGM-3 gravimeter [*Bell and Watts*, 1986]. The meter output (counts) are acquired at 1-s intervals, converted to acceleration and smoothed with a 180-s Gaussian filter to remove ship motions. These total field measurements are then sampled at 1-min intervals, merged with the Global Positioning System (GPS) navigation to determine the Eötvös correction and the free-air anomalies calculated by removal of the predicted gravity at the measurement latitude using the 1967 International Gravity Formula. Since most applications of shipboard gravity data use spatial rather than temporal dimensions, we used an Akima spline to resample the data at 0.2-nautical mile (370 m) intervals.

The gravity data resulting from this standard processing are characterized by 2-5 mGal variations with wavelengths of a few kilometers (Figure 6a). This short-wavelength noise, which can not be due to sources at or below the seafloor, is characteristic of marine gravity data collected with BGM-3 gravimeters. The spectrum of our resampled data is linear at wavenumbers of less than 0.1 km^{-1} (wavelengths > 10 km) (Figure 6b), as is typical of marine gravity spectra. At higher wavenumbers (shorter wavelengths), the spectrum is much flatter, representing a noise floor. We attempted to remove the short-wavelength noise by designing a digital low pass filter to retain all wavelengths greater than 10 km at full power and roll off to full stop by 5 km (C. Small, manuscript in preperation). The spectrum of the filtered data is shown in Figure 6b, and the filtered and unfiltered data can be compared in Figure 6a. Application of the filter resulted in a significant improvement of crossover errors with the mean crossover error reduced from 2.0 mGal to 1.1 mGal.

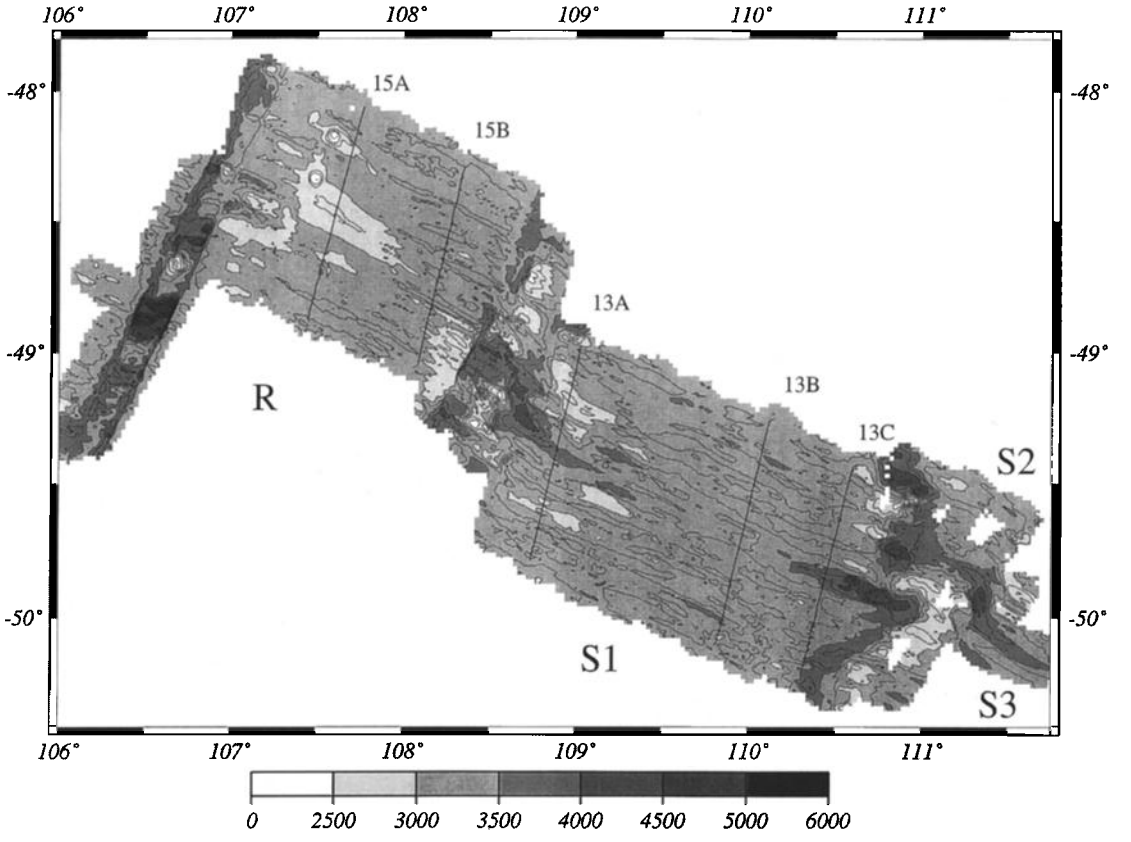

Figure 4. Bathymetric map of detailed survey box 2 (Figure 1). The bathymetry is contoured at 250-m intervals, and shading changes occur at 500-m intervals. The detailed survey extends out to approximately 1.2 Ma seafloor on both flanks. Solid lines show the location of center beam bathymetry and free-air gravity profiles shown in Figures 13 and 15 (15A, 15B, 13A, 13B, 13C). The map includes segments R, S1, S2, and S3 (Figures 7 and 8). The ridge axis for 50 km near the center of segment R is a narrow volcanic ridge on top of a 20-km-wide fault bounded plateau. The plateau dies away at both ends of the segment where the axis is within a shallow axial valley. Short segment S2 has nearly been cut off by the propagating rift at the eastern tip of S1.

The Southeast Indian Ridge

The SEIR forms the plate boundary between the Australian and Antarctic plates from the Indian Ocean Triple Junction located near 25°S, 70°E to the Macquarie Triple Junction near 63°S, 165°E. Rifting between Australia and Antarctica began in the Late Cretaceous with slow seafloor spreading beginning by about 96 Ma [*Cande and Mutter*, 1982; *Veevers*, 1986]. The SEIR has been spreading at intermediate rates of about 55-75 mm/yr since the Oligocene (Anomaly 13) [*Royer and Sandwell*, 1989]. Present-day spreading rates increase rapidly from 57.5 mm/yr at the Indian Ocean Triple Junction to 68 mm/yr at Amsterdam and St. Paul Islands and then more slowly to a maximum of 76 mm/yr near 50°S, 114°E, before decreasing gradually to 72 mm/yr at the George V fracture zone near 50°S, 139°E [*DeMets et al.*, 1990]. Spreading rates in the survey area are nearly constant at 72-76 mm/yr, within the range of 70-80 mm/yr where the transition from an axial high to an axial valley is observed to occur [*Small and Sandwell*, 1989; *Macdonald*, 1986; *Malinverno*, 1993].

Satellite altimetry data [*Small and Sandwell*, 1994] and the sparse pre-1995 shipboard data from the SEIR [*Cochran*, 1991; *Ma and Cochran*, 1996] show that transitions from axial lows to axial highs occur at a number of places on the SEIR, specifically near 82°E, near 101°E, and near 127°E at the eastern boundary of the Australian-Antarctic Discordance (AAD). The change in axial morphology near 101°E from an axial high toward the west to an axial valley toward the east is of particular interest because it occurs well away from anomalous features such as hot spots or the AAD in an area where the spreading rate is nearly constant.

There is, however, a significant depth gradient across the region (Figure 7) with axial depths increasing from about 2300 m near 88°E to nearly 4500 m east of 114°E near the AAD [*Ma and Cochran*, 1996]. Ridge flank depths increase by about 500 m from 2800 m to 3300 m over the same region. [*Ma and Cochran*, 1997]. *Forsyth et al.* [1987] determined that the shear wave velocity beneath the AAD is considerably faster than for similar age mantle in other parts of the SEIR and the Pacific, which can be interpreted to result from colder than normal mantle in that region. Major element chemistry implies shallower and smaller extents of melting beneath the AAD than in adjacent areas, also suggesting the presence of colder mantle beneath the AAD [*Klein et al.*, 1991; Pyle, 1994]. This is further supported by interpretation of gravity data [*West et al.*, 1994] and by recent seismic refraction results from the AAD which show thin crust (4.2 km), indicating a low melt supply consistent with a colder than average mantle [*Tolstoy et al.*, 1995]. The SEIR between 88°E and 120°E thus presents the opportunity to conduct a "controlled experiment" in which the effects on the crustal accretion processes of vary-

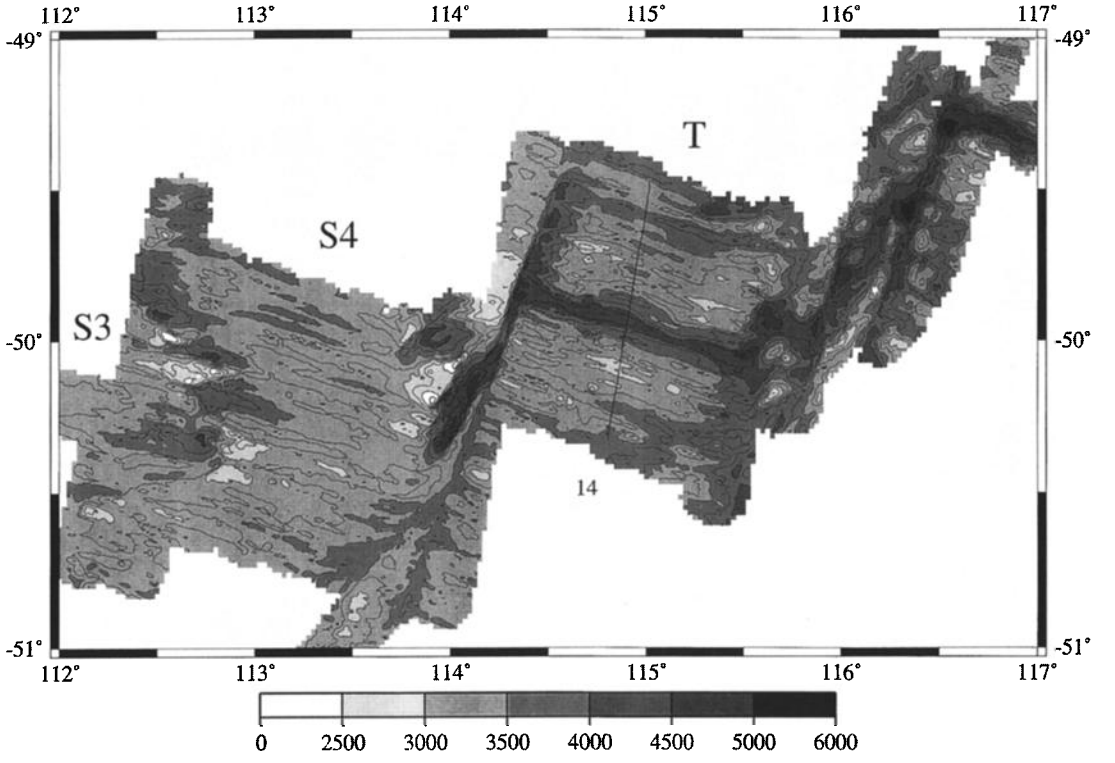

Figure 5. Bathymetric map of detailed survey box 3 (Figure 1). The bathymetry is contoured at 250-m intervals, and shading changes occur at 500-m intervals. The detailed survey extends out to approximately 1.2 Ma seafloor on both flanks. Solid lines show the location of the center beam bathymetry and free-air gravity profiles shown in Figure 14. The map includes segments S4 and T, as well as the eastern end of S3 (Figures 7 and 8). The axial morphology changes from a shallow valley to a deep valley across the 114°E transform, which appears to form the effective western boundary of the AAD. An eastward propagating rift has recently stalled just west of the 114°E transform and has cut an en echelon series of shears to reach the transform. The recently eliminated ridge tip can be identified near 50°S, 114°E.

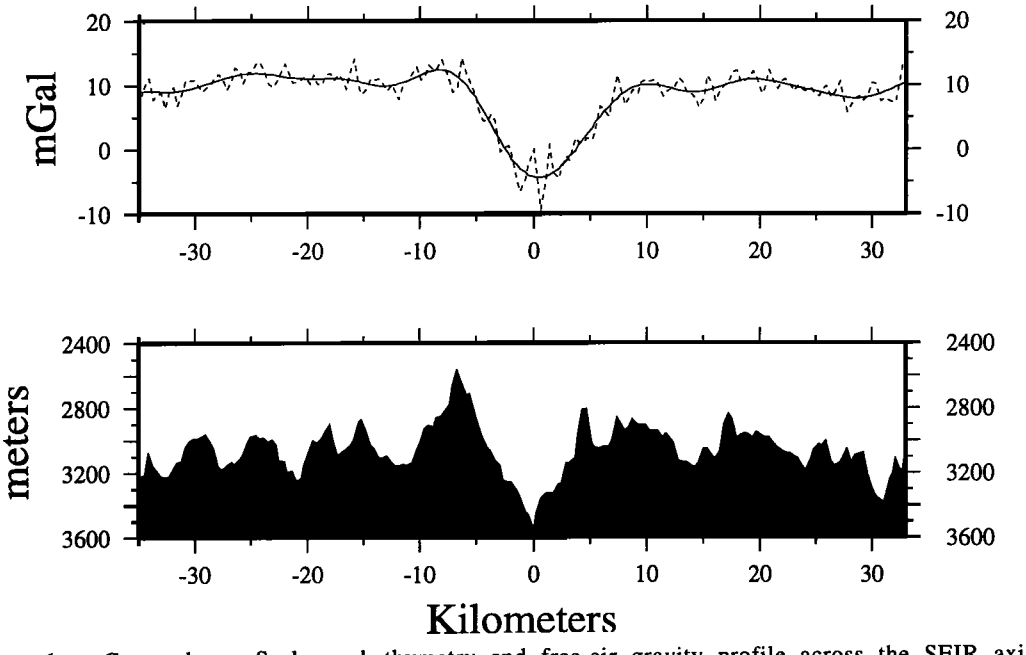

Figure 6a. Center beam Seabeam bathymetry and free-air gravity profile across the SEIR axis at 105°33.1'E. The dotted gravity curve shows the raw (unfiltered) data. The solid curve shows the same data after application of the filter shown in Figure 6b to remove short-wavelength noise.

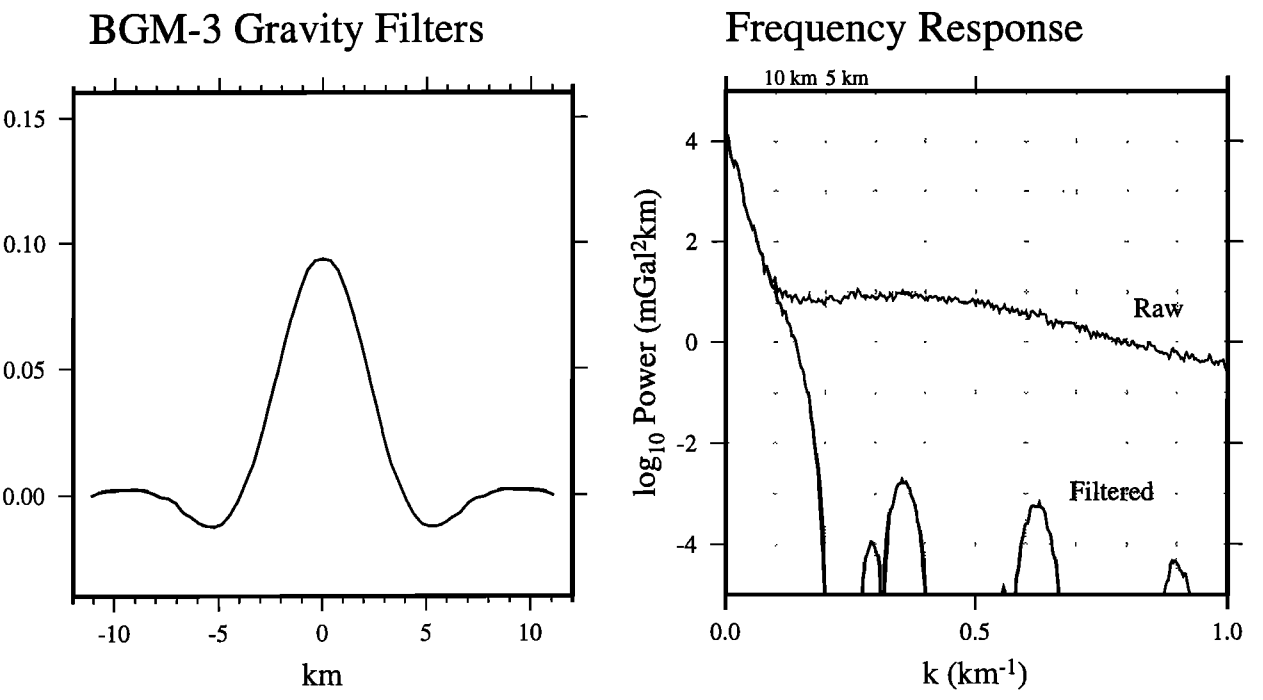

Figure 6b. (left) Filter convolved with free-air gravity data to remove short-wavelength noise. Filter fully retains all wavelengths greater than 10 km and rolls off to full stop at 5 km. (right) Spectra of the raw and filtered free-air gravity data. The filter removes the "noise floor" present at wavelengths shorter than 10 km in the raw data.

ing the mantle temperature at a constant spreading rate can be examined.

The first-order segmentation of the SEIR as determined by C. Small et al. (The structure and segmentation of the Southeast Indian Ridge, submitted to *Marine Geology*, 1997) is shown in Figure 8. The letter names assigned to the segments continue the convention established by *Royer and Schlich* [1988] for the portion of the SEIR from the Rodriques Triple Junction to Amsterdam Island and extended by *Johnson et al.* [1996] to the region from Amsterdam Island to 88°E. There are eight-first order segments in the survey area which range in along-axis length from 55 km (segment N) to over 700 km (segment M). Segment boundaries were determined by mapping stable, long-lived fracture zone traces in satellite gravity data (C. Small et al., submitted manuscript, 1997) All of the first-order segment boundaries are marked by transform faults with present-day offsets of 37 to 130 km.

The first- and second-order ridge segmentation is also indicated on Figure 7. The second-order segments are less stable over time, and in several cases the nontransform offsets bounding them appear to be propagating to the east. The eastern boundaries of segments M3, M5, S1, and S3 are all propagating to the east (Figures 4, 5, and 9). A propagating rift which formed the eastern boundary of segment S4 has recently collided with the 114°E transform. The remnants of the eliminated ridge segment can be seen just west of the 114°E transform near 50°S (Figure 5). The boundary between segments P3 and P4 also consists of propagating rifts, but here the propagation appears to be oscillatory or "dueling," so that there has been little net motion since 1 Ma (Figure 3).

Morphology of the Southeast Indian Ridge Axis

An along-axis profile of axial depth on the SEIR from 89.5°E to 115.5°E is shown in Figure 7. The profile was constructed by digitizing the location of the ridge axis at 1 arc min (~ 1.2 km at this latitude) intervals of longitude on detailed Seabeam maps and extracting the depth at those locations from the gridded bathymetry. The along-axis depth profile in Figure 7 confirms the general increase in axial depth from west to east determined from older widely spaced tracks [*Ma and Cochran*, 1996]. These data also confirm the observation made by *Ma and Cochran* [1996] that the rate of axial deepening increases to the east of about 100°E. Axial depths increase gradually from about 2400 m to about 2800 m between 89°E and 102°E and then more steeply to about 3700 m near 113°E. There is a sharp, step-like increase in the axial depths to about 4500 m across a transform fault at 114°E which marks the transition from a shallow to a deep rift valley.

The along-axis depth profile in Figure 7 also shows that the increase in axial depth is not monotonic. At an intermediate scale of 300-500 km the eastward increase in depth is modulated by the major long-lived transforms. Axial depths become shallower by a few hundred meters from west to east across transforms at 96°E, 100°E, and 106°30'E and deepen by nearly 1000 m across the transform at 114°E.

The along-axis variation in ridge flank depths [*Ma and Cochran*, 1997] is much less than the variation in axial depth (~500 m rather than ~2100 m) (Figure 7) which is to be expected since the axial depth reflects not only the change in the depth of the ridge but also changes in the form and relief of the axial topography. The ridge flank depths also appear to vary more smoothly and continually than the axial depths. However, we can only determine ridge flanks depth for the eight segments for which we possess significant off-axis data (Figures 2-5). Thus we can not determine whether is a step in ridge flank depths across the transforms at 96°E, 100°E, and 106°30'E. Ridge flank depths do not change significantly across the transform at 114°E in spite of the 1000 m change in axial depth (Figures 5 and 7).

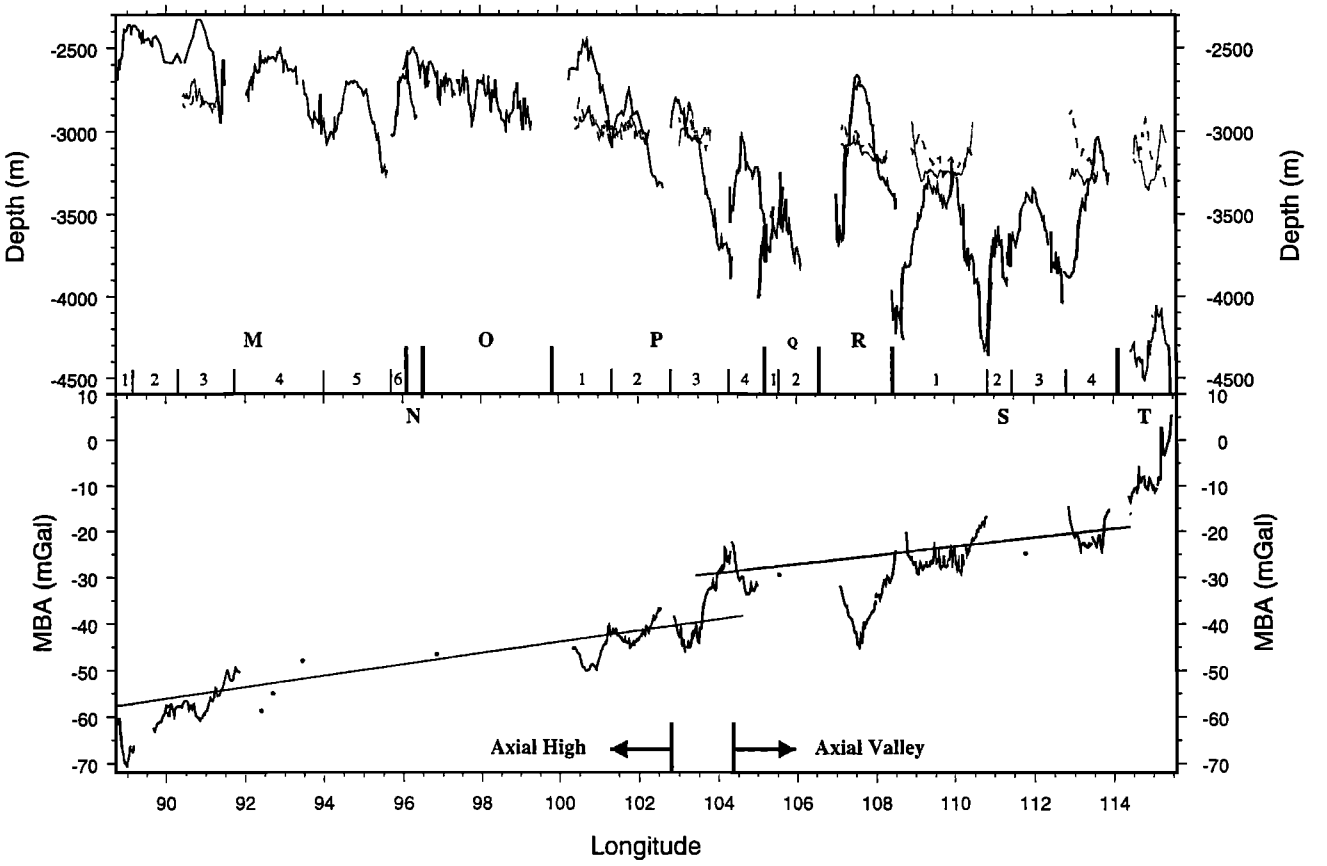

Figure 7. (top) Axial and ridge flank depth as a function of longitude along the SEIR. The axial depth profile, shown as a heavy solid line, was constructed by digitizing the location of the ridge axis at 1 arc sec (~ 1.2 km) longitude intervals on detailed Seabeam maps and extracting the depth at those locations from the gridded bathymetry. The ridge flank depths, shown as light lines (solid for the north flank and dashed for the south flank) for the eight segments contained within the detailed study boxes, were determined by *Ma and Cochran* [1997] from the deterministic component of an empirical orthogonal function analysis of the bathymetric data. Axial depth increases from west to east from 2350 m in segment M1 to 4000-4500 m in segment T. The accompanying change in ridge flank depth is ~500 m (2800-3300 m). First- and second-order segmentation of the axis of the SEIR is shown along the bottom. (bottom) Axial mantle Bouguer anomaly (MBA) as a function of longitude along the SEIR. Within the four detailed study boxes, the gridded MBA gravity was sampled at 1.2-km intervals along the ridge axis. Between detailed survey boxes, spot values (dots) were obtained where the ship track crossed the ridge axis. Thin solid lines show the regional trend. Note the abrupt steps in the axial MBA level near 104°E and 115°E, which correspond to changes in axial morphology.

There is also a segment scale (~100 km) axial depth variation superimposed on the longer-wavelength pattern. The ridge axis is generally shallowest toward the center of segments with axial depths increasing toward segment bounding offsets. This type of segment scale depth variation is also observed at both fast and slow spreading ridges and appears to be in large part related to segment scale upwelling and melt distribution [*Macdonald et al.*, 1988, 1991; *Sempere et al.*, 1990; *Lin et al.*, 1990]. Intrasegment axial depth variations are generally less than 500 m to the west of 103°E but may be as great as 1000 m in segments bounded by propagating rifts and in two segments (P3 and R) in which there is a change from axial high to valley within the segment.

Satellite altimetry data suggest that a change from an axial high to an axial valley occurs on the SEIR between 100°E and 105°E [*Small and Sandwell*, 1992]. The shipboard survey determined that the transition occurs within segment P3 which extends from 47°43'S, 102°52'E to 48°11'S, 104°22'E (Figures 3 and 7). All segments for 1900 km west of 103°E to 81°E near Amsterdam Island are characterized by axial highs (Figures 2, 3 and 10). The only exception is segment N, a 55-km-long segment near 95°45'E, bounded at both ends by transforms with offsets of 93 and 37 km, which has a 200-500 m deep valley at its axis (Figure 9). All segments for 1450 km east of 104°30'E to the eastern boundary of the AAD at 129°E are characterized by axial valleys (Figures 4, 5, and 11-14). There is again a single exception to this pattern. For about 50 km in the center of segment R, located immediately to the east of the 130 km offset 106.5°E transform, the axis is formed by a linear volcanic ridge along the apex of a broad fault-bounded plateau (Figures 4 and 15). The plateau becomes less distinct to the east and the eastern end of the segment has a shallow axial valley (Figure 15).

Although a transition from an axial high to an axial valley can be defined near 103°30'E, the transition is not between well-developed, end-member morphologies. Both "East

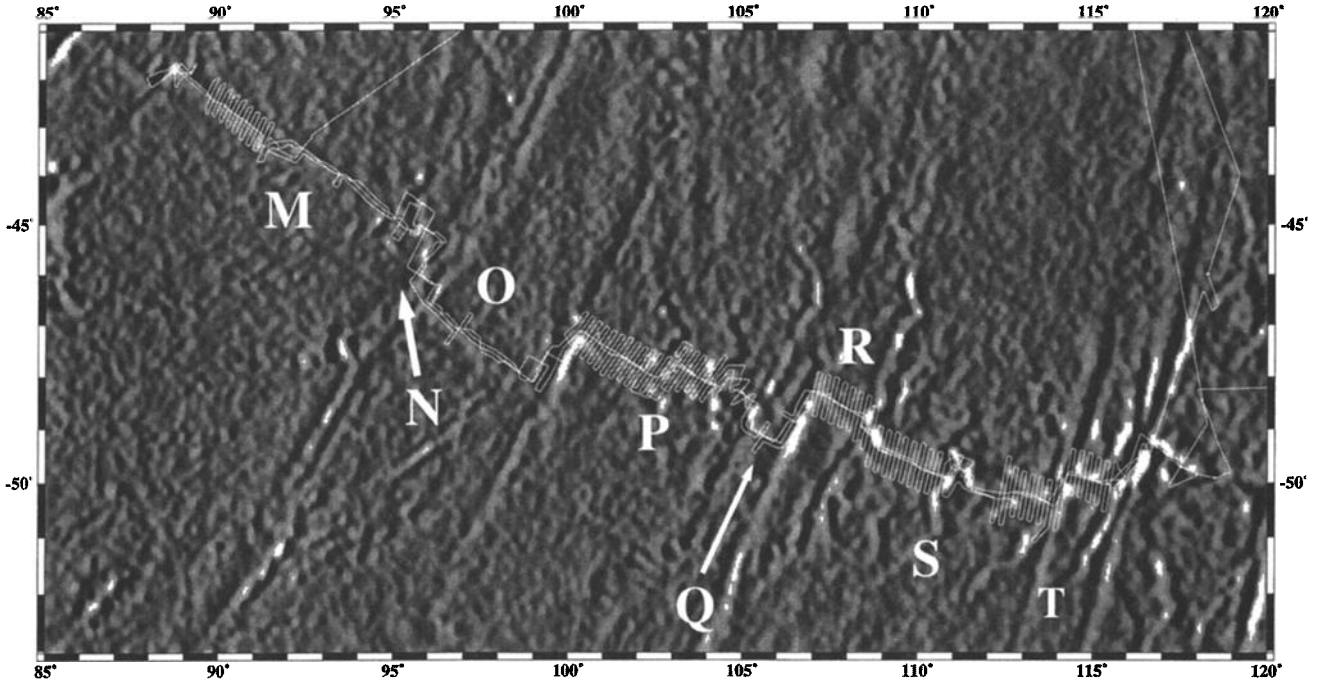

Figure 8. First-order segmentation of the SEIR superimposed on a band-passed satellite gravity image. Survey tracks of the Westward 9 and 10 cruises of R/V *Melville* are shown in white. The first-order segmentation was established by C. Small et al. [submitted manuscript, 1997] through identification of stable long-lived segment boundaries in satellite gravity images. Figure is from C. Small et al. [submitted manuscript, 1997].

Pacific Rise-type" axial highs and deep "Mid Atlantic Ridge-type" rift valleys do exist on the SEIR, but they are found only in a few specific areas. Well-developed deep rift valleys (> 1000 m deep) occur only to the east of the 114°E transform (Figures 5 and 14). The change in morphology across the 114°E transform is quite dramatic (Figure 5), and the transform appears to mark the effective western boundary of the AAD. Axial valleys on the SEIR to west of 114°E are generally < 500 m deep (Figures 4, 5, and 11-13) except near segment ends where they may deepen to 700 m or to about 1000 m at propagating rift tips (Figures 4, 5, and 13).

Well-developed axial highs similar to those characteristic of the EPR are found only in segments S1 and S2 immediately east of the 88°E transform (Figure 2) and in the central portion of segment P1 immediately to the east of the 100°E transform (Figures 3 and 10). Otherwise, axial highs on the SEIR are "rifted highs" which are lower and less well defined and are characterized by faults with throws of 50-100 m very near the axis, often within about 1 km (Figure 10). The eastern end of S2 and both ends of P1 also more rifted.

Shallow rift valleys and rifted highs thus appear to form a distinctive and characteristic intermediate rate axial morphology which is prevalent on the SEIR. These morphologies differ from the well-studied, end-member morphologies not only in the amplitude of the axial relief but also in the nature of the neovolcanic zone. Faulting is evident throughout the axial region in areas with these morphologies, and in many areas a traditional morphologically defined neovolcanic zone is not evident. In fact, the axis can not always be accurately defined on the basis of morphology alone.

Gravity Anomalies at the Southeast Indian Ridge Axis

Free-air and mantle Bouguer gravity anomaly maps of the four detailed study boxes, contoured at 5 mGal intervals are shown in Figures 16-19. The free-air anomaly maps were constructed by gridding the filtered shipboard gravity data on a 1.5 arc min x 1 arc min (~1.8 km x 1.8 km) grid and fitting a smooth surface using a continuous curvature spline in tension [*Smith and Wessel*, 1990; *Wessel and Smith*, 1995]. For calculation of mantle Bouguer anomalies the gravity effect of the topographic and the assumed Moho relief were determined from gridded bathymetric data using the technique of *Parker* [1973], retaining four terms in the series expansion. A constant crustal thickness of 6 km was assumed with density contrasts of 1700 and 600 kg/m^3 assumed across the water/crust and crust/mantle interfaces respectively. A 0.5 arc min x 0.5 arc min (~600 m x 900 m) topographic grid was used in the calculations. The grids of the gravity effects of the topographic and assumed Moho relief were sampled at the locations of the shipboard measurements and the values obtained at those locations subtracted from the coincident shipboard free-air gravity anomalies. The resulting MBA anomalies were then gridded and contoured in a manner identical to that used for the free-air gravity.

Free-Air and Mantle Bouguer Anomalies

Free-air anomalies on the ridge flanks away from large topographic features are generally in the range of -5 to 10 mGal and only exceed ±30 mGal over the largest topographic

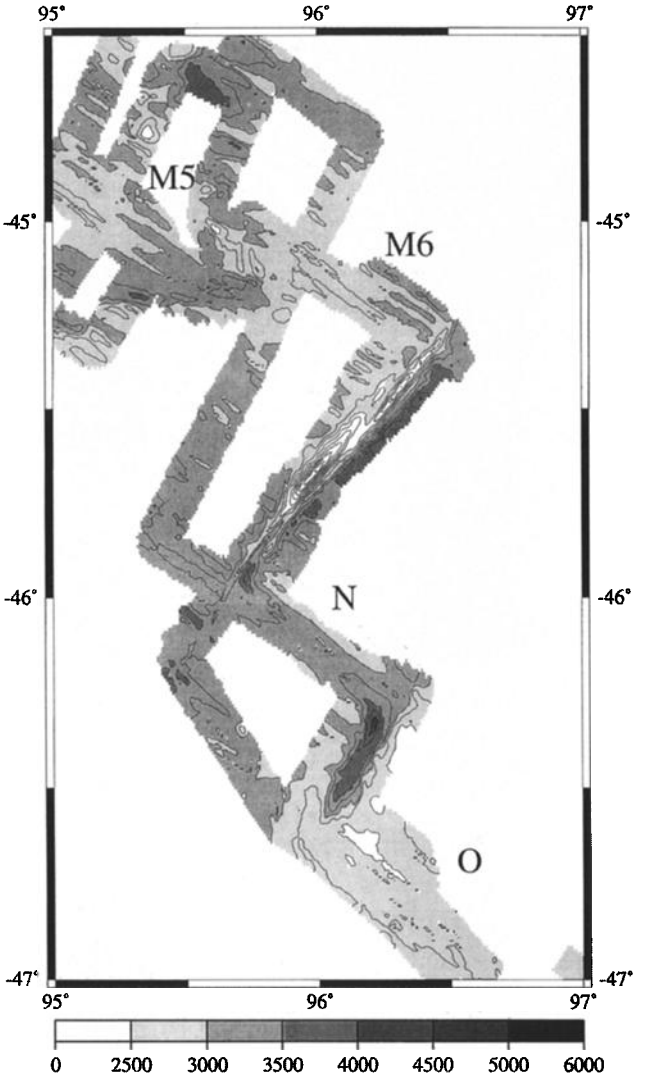

Figure 9. Bathymetric map of the SEIR ridge axis from 95°E to 97°E. The bathymetry is contoured at 250-m intervals and shading changes occur at 500-m intervals. The map shows the ridge axis at the southeastern end of segment M5, all of segments M6 and N, and the northwestern end of segment O. Segment N, which extends for 55 km between two transforms, is the only segment between 82°E and 104°E characterized by an axial valley morphology. The M5 ridge axis is propagating to the southeast.

features. The largest positive free-air anomaly measured in the survey area (78 mGal) is found over a fracture zone ridge near 96°E (Figure 9) which reaches to within 700 m of the surface and appears to be slightly oblique to the spreading direction, so that it is under compression [*Sempere et al.*, this issue]. Free-air gravity anomalies of 55-65 mGal were also measured over three large seamounts at the very western end of the survey area at 41°53'S, 88°09'E; 41°45'S, 89°16'E; and 43°23'S, 91°17'E (Figures 2 and 16). The largest measured negative anomaly (-61 mGal) is at 49°55'S, 106°35'E over the deep (4800 m) pull-apart basin within the 106.5°E transform (Figures 4 and 18). Free-air anomalies of -50 to -60 mGal were also measured in three deep basins within the complex 116°E transform (Figures 5 and19).

The free-air anomalies generally reflect the topographic relief. Most of the smaller-scale features related to bathymetric relief in the free-air anomalies are removed in the MBAs which thus appear much smoother at the 5-mGal contour interval of our maps (Figures 16-19). The three large seamounts in the western survey box show 5-10 mGal MBA lows (Figure 16) reflecting isostatic support through crustal flexure resulting in slightly thicker crust underneath the seamounts. The large free-air anomalies over transforms are almost entirely removed by the topographic correction. For example, the very complicated free-air anomalies associated with the combination transform/non-transform ridge offset at 108.5°E (Figure 18) are replaced in the MBA map by a simple gravity high trending along the spreading direction in which individual bathymetric features cannot be identified. In general, transforms appear as 10-15 mGal MBA gravity highs probably reflecting thinned crust beneath the transforms [*Prince and Forsyth*, 1988].

Gravity Anomalies Over Propagating Rifts

A distinctive pattern of free-air anomalies is found at the propagating rifts at 111°E and 112°45'E (Figures 18 and 19). Prominent -25 to -35 mGal free-air anomaly lows are located over both the propagating and retreating rift tips and over a series of abandoned rift tips along the inner pseudofaults. Large-amplitude (25 to 30 mGal) positive anomalies are found associated with blocky topographic highs located between the propagating and retreating rift tips and with similar features which appear to be their fossil equivalents along the inner pseudofault. The outer pseudofaults appear as linear bands of positive and negative free-air anomalies with a relief of ~30 mGal (Figures 18 and 19). This is particularly clear for the 111°E propagating rift which is well exposed on the southern ridge flank in our survey (Figures 4 and 18). The crust created at retreating rifts appears to be uplifted by 200-400 m along the outer pseudofaults, which are marked by scarps facing toward the crust created at the propagating rift. A shallow trough extends along the base of the scarp. The free-air anomalies at the outer pseudofaults are largely removed by the topographic correction. The outer pseudofaults at the 112°45'E and 114°E rifts are not apparent in the MBA map (Figure 19). There is a 10 mGal MBA high over part of the 111°E outer pseudofault (Figure 18), but it is at the very edge of the survey and may represent an artifact. The inner pseudofaults appear in the MBA maps as linear ~10 mGal positive anomalies.

Gravity Anomalies Over the SEIR Axis

The ridge axis at segments with an axial high, whether EPR-like, rifted, or anomalous (segment R), is marked by a 10-15 mGal free-air anomaly high. The axial gravity high is best developed where the ridge crest bathymetric high is well developed and appears magmatically vigorous (i.e., less faulted), usually near the center of segments (Figures 10, 16 and 17).

The EPR-like segments, M1, M2, and P1, show a characteristic "bull's eye" pattern with MBA lows of 10 to 15 mGal centered over the most vigorous portion of the segment. The along-axis half-segment MBA gradient (as defined by *Lin and Phipps Morgan* [1992]) for segment P1 is 0.24 mGal/km (Figure 17b), which is similar to those observed at the fast spreading EPR [*Wang and Cochran*, 1993, 1995].

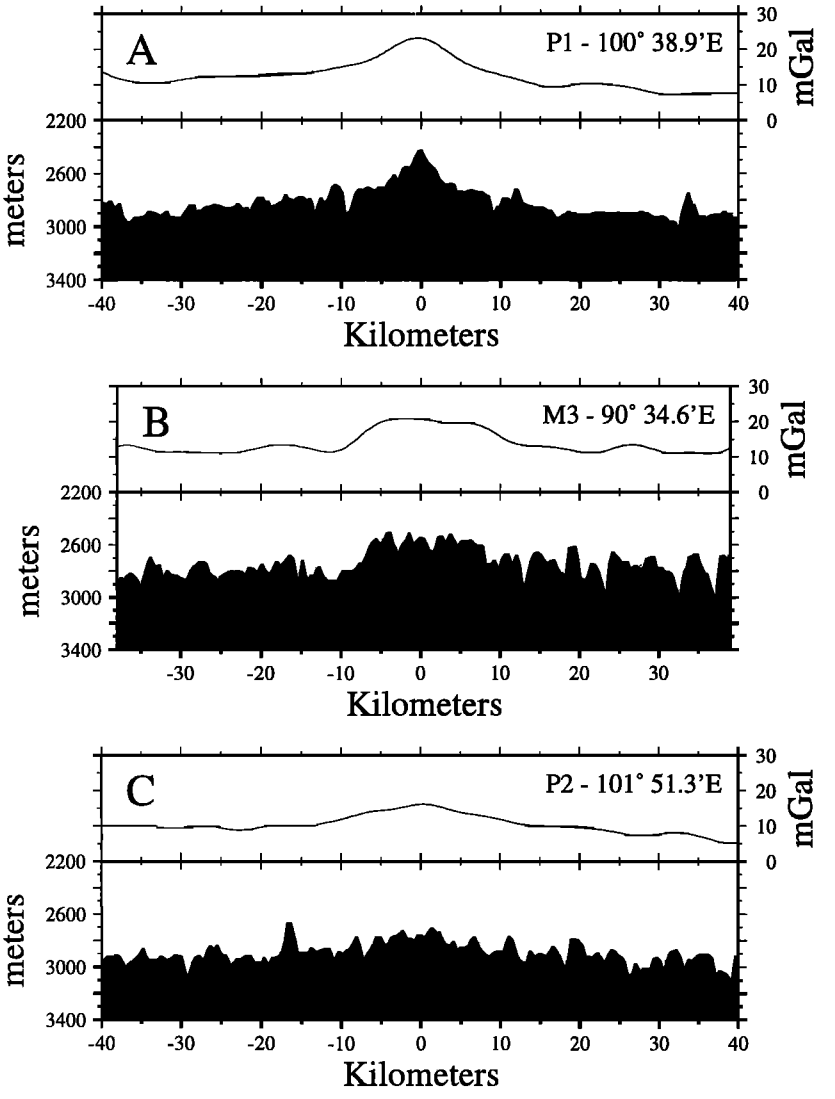

Figure 10. Center beam Seabeam bathymetry and free-air gravity profiles across the SEIR axis illustrating observed axial high morphologies. The location of the profiles is shown in Figures 2 and 3. Profiles have been projected perpendicular to the axis which is located at 0 km on the horizontal scale. The ridge axis was located on the basis of an axial magnetic anomaly high. The longitude at which the profiles cross the ridge axis is shown on each profile along with the segment in which it is located. The northern ridge flank is to the right. Well-developed "EPR-like" axial highs (Figures 10a) are only observed immediately east of left-stepping transforms at 88°E and 100°E. Otherwise rifted axial highs (Figures 10b and 10c) are the characteristic axial morphology from 82°E to 103°E.

The two rifted high segments (M3 and P2) included in our detailed survey boxes also have MBA lows over the center of the segment, but these are not as pronounced as at the more vigorous segments (Figures 16 and 17). The half-segment gradients for these two segments are 0.10-0.14 mGal/km which is at the low end of the range generally observed at segments with axial highs [*Wang and Cochran*, 1995].

Thus vigorous EPR-like segments are marked by along-axis MBA gradients similar to those observed at the EPR. The rifted high segments have lower gradients away from major ridge offsets, although they are still characterized by small MBA lows centered over vigorous, apparently volcanically active portions of segments.

Most of the region between 104°E and 114°E is characterized by a shallow axial valley (Figures 4, 5 and 11-13), including all of 165-km-long segment S1 (~108°40'E to 110°45'E) (Figure 4). The axial valley has a relief of about 1000 m at both ends of the segment near the 108°40'E nontransform offset and the 110°45'E propagating rift. However, the axial valley shoals rapidly away from both of these features and has a depth of < 600 m from about 109°E to 110°25'E (Figures 4 and 13). The axis is marked by a free-air anomaly minimum with an amplitude proportional to the depth of the valley (Figures 13 and 18). Near the ends of the segment, the free-air minimum is about 40 mGal but decreases to a subtle 3 mGal low near 109°55'E where the axial valley becomes so shallow as to be almost unrecognizable on across-axis profiles (Figures 4 and 13).

In spite of the great along-axis variation in axial relief and in free-air gravity anomalies, mantle Bouguer anomalies

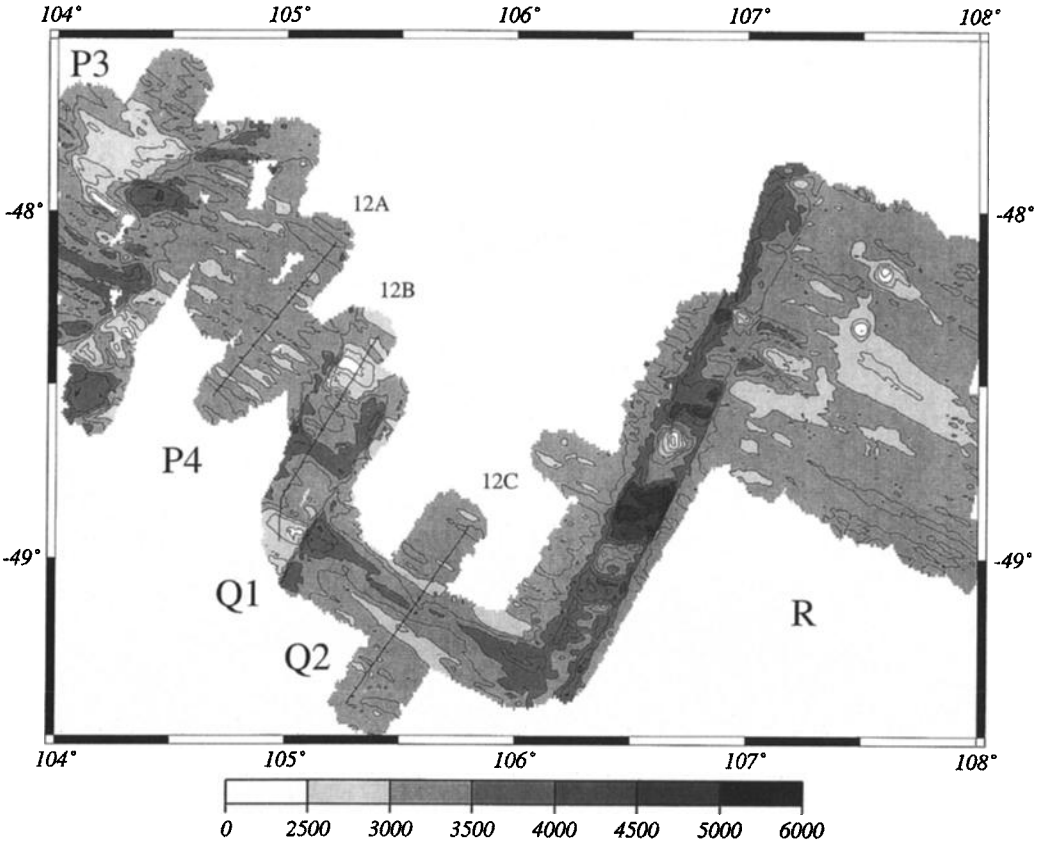

Figure 11. Bathymetric map of the SEIR ridge axis from 104°E to 108°E. The bathymetry is contoured at 250-m intervals, and shading changes occur at 500-m intervals. The map shows the ridge axis at the southeastern end of segment P3, all of segments P4, Q1, and Q2, and the northwestern end of segment R. The location of gravity and center-beam bathymetry profiles across the axis from segments P4, Q1, and Q2 shown in Figure 12 (12A, 12B, and 12C) are indicated.

within segment S1 show very little along-axis variation away from the segment boundaries. Axial MBA gravity values vary by less than 3 mGal for a distance of 110 km from 108°50'E to 110°14'E in spite of the fact that axial depth varies by about 450 m along this portion of the ridge (Figure 18) and the axial morphology changes from a 600-m-deep valley to a practically flat axial profile and back to a 400-m-deep valley (Figure 4). Axial MBAs do increase by 10 mGal over the eastern 50 km of the segment as the axial depth increases by ~1000 m toward the 111°E propagating rift. This probably reflects a decrease in crustal thickness toward the propagating rift.

A similar lack of correspondence between axial depth and mantle Bouguer anomalies is evident in segment S4. In this segment the axial depth decreases steadily from ~3900 m at the retreating rift tip near 112°55'E to ~3000 m at 113°37'E (Figure 5 and 19). As a result, the axial valley, which is 700 m deep at the western end of the segment, becomes steadily shallower until it evolves into a narrow, 150-m-high volcanic ridge for a few km near 113°37'E. There are very steep MBA gradients in the immediate vicinity of the 108°45'E retreating rift tip and the 114°E transform, again probably reflecting crustal thinning near those discontinuities. However, for 50 km from 113°05'E to 113°44'E, there is less than 3 mGal variation in the MBA values This region of flat MBA gravity encompasses 700 m of relief in axial depth and the entire range of axial morphologies.

The shallow valley morphology on the SEIR thus appears to be characterized by a lack of correspondence between axial depth and axial MBA values and by nearly constant axial MBA values away from major ridge offsets. This differs from the pattern normally observed at ridge segments with either axial highs or deep axial valleys which both generally show well-defined minima associated with the shallowest or most vigorous portion of the segment. The axial depth variation observed in the central portion of segments S1 and S4 must be created and maintained by a non-isostatic mechanism and be related to ridge axis dynamics since it is not observed on the ridge flanks.

The deep axial valley to the east of the 114°E transform (Figure 5) is marked by large-amplitude free-air anomalies (Figures 14 and 19) with across-axis relief of ~60 mGal. Both the bathymetry and the free-air anomalies show a distinct asymmetry across the axis such that the rift mountains and the free-air gravity anomalies over them are higher to the north at both ends of the segment and to the south in the center of the segment. The asymmetry does not appear to represent an "inside corner" effect [*Tucholke and Lin*, 1994], particularly at the western end of the segment, where the asymmetry is of the opposite sense.

Although the 115°E segment closely resembles typical MAR segments on across-axis bathymetry and gravity profiles (Figure 14), along-axis depth and gravity profiles do not re-

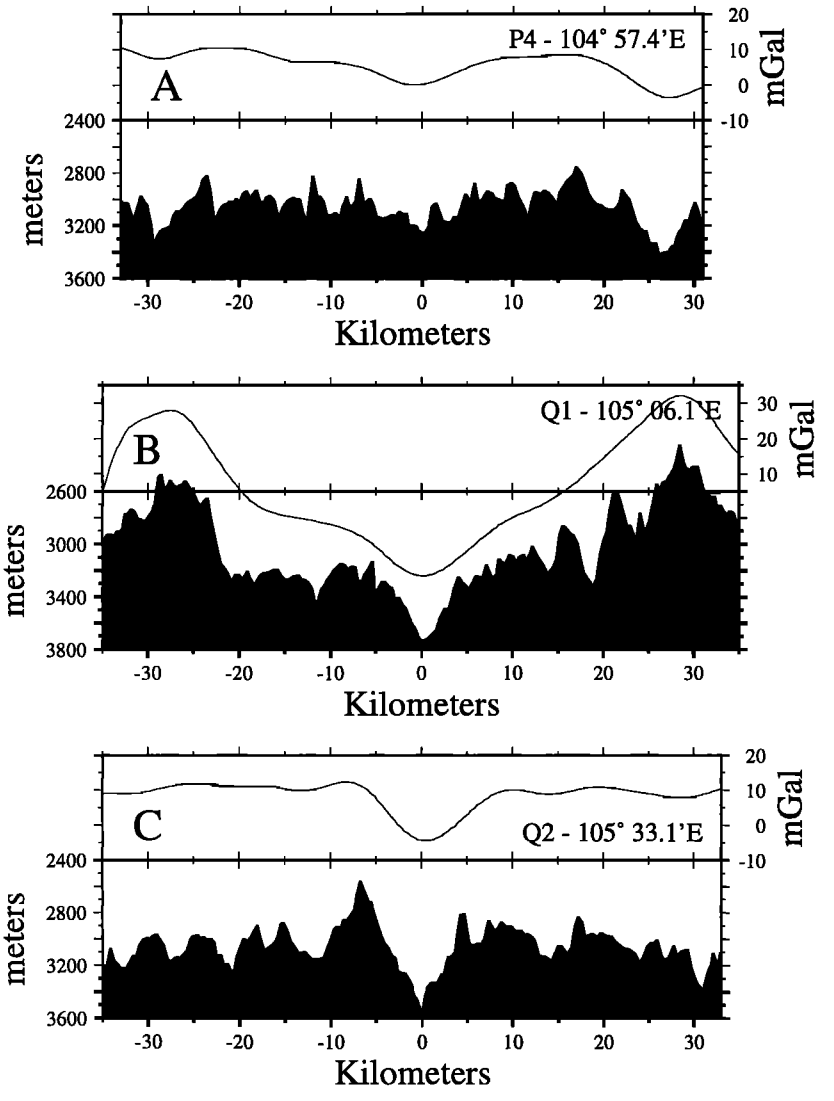

Figure 12. Center beam Seabeam bathymetry and free-air gravity profiles across the SEIR axis from segments P4 (a), Q1 (b), and Q2 (c) where the axis is characterized by a shallow valley. The location of the profiles is shown in Figure 11. Profiles have been projected perpendicular to the axis which is located at 0 km on the horizontal scale. The ridge axis was located on the basis of an axial magnetic anomaly high. The longitude at which the profiles cross the ridge axis is shown on each profile along with the segment in which it is located. The northern ridge flank is to the right. Segments P4, Q1, and Q2 are the first segments to the east of the change in axial morphology which occurs between 103°E and 104°30'E.

semble those observed at the MAR [e.g., *Lin et al.*, 1990; *Sempéré et al.*, 1993; *Detrick et al.*, 1995]. The axial depth profile is nearly flat in the western third of the segment (Figure 19b), so that the deepest portion of the axial valley is at 114°47'E near the center of the segment rather than at the bounding offsets. Axial mantle Bouguer anomalies increase away from rather than toward the 114°E transform. However, the axial mantle Bouguer anomalies do roughly mirror the axial depth with a local MBA high at the depth maximum near 114°47'E and a local low at the depth minimum near 115°06'E (Figure 19).

The two segments, P3 at 104°E and R at 108°E, in which a transition occurs between an axial high and an axial valley (Figures 4 and 5), both show distinct MBA bull's eye lows with large along-axis gravity gradients. This pattern is best developed at segment R (Figure 18). An MBA minimum is located over the shallowest point on the axis at 48°27'S, 107°35'E. MBA gravity increases along-axis by 12.5 mGal with a gradient of 0.35 mGal/km to the west as the depths plunge by 950 m over a distance of 36 km toward the 106.5°E transform. The MBA axial gravity also increases eastward from the depth minimum by 20.4 mGal over 78 km (0.26 mGal/km) as axial depths increase by 770 m toward the 21 km-offset 108°45'E ridge discontinuity. The steep axial depth and MBA gradients away from 107°35'E appear to imply a vigorous melt supply centered at that location. This is supported by the presence of a chain of large seamounts extending away from the depth minimum on the northern ridge flank (Figure 4). However, off-axis ridge flank depths do not show a minimum near the center of the segment but rather vary continu-

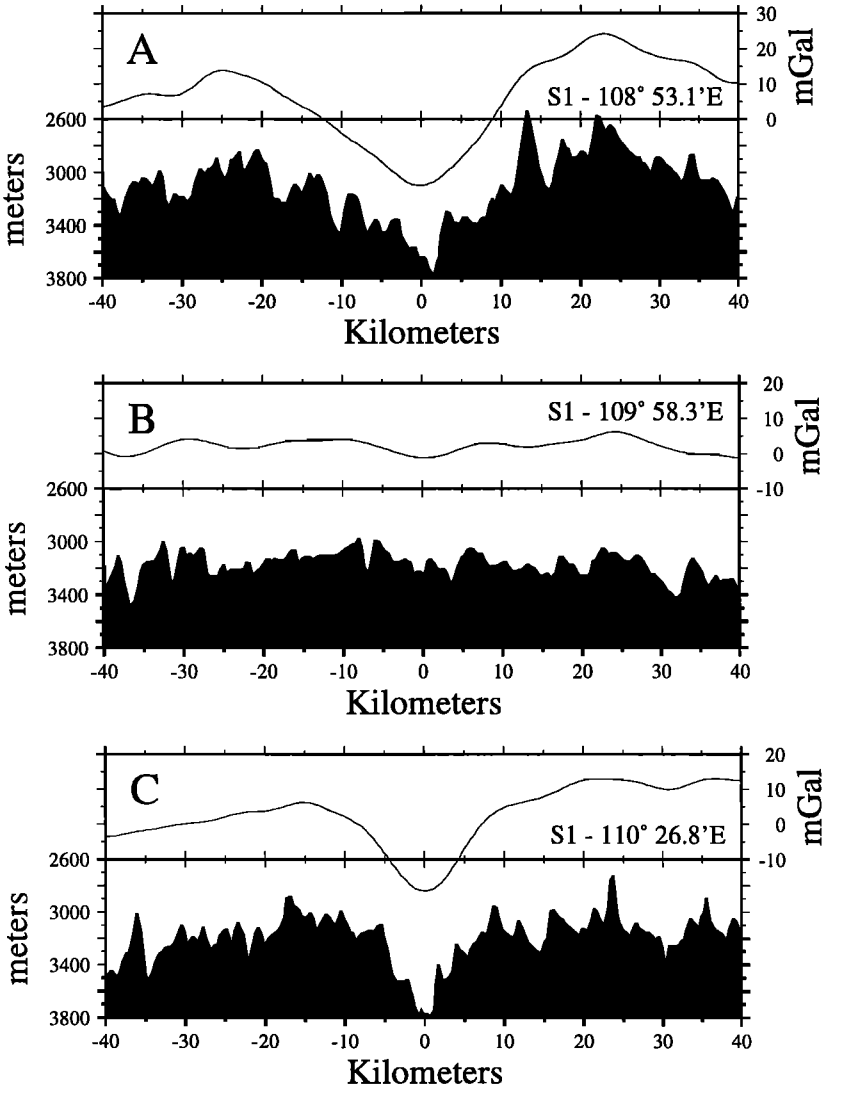

Figure 13. Center beam Seabeam bathymetry and free-air gravity profiles across the SEIR axis from segment S1 which is characterized by an axial valley. The location of the profiles is shown in Figure 4. Profiles have been projected perpendicular to the axis which is located at 0 km on the horizontal scale. The ridge axis was located on the basis of an axial magnetic anomaly high. The longitude at which the profiles cross the ridge axis is shown on each profile along with the segment in which it is located. The northern ridge flank is to the right. The 165-km-long segment is characterized by an axial valley for it entire length. The valley is about 1000 m deep near the complex transform/nontransform offset at its western end and the propagating rift at its eastern tip (Figures 13a and 13c). However, the axis shallows rapidly away from its extremities, and the axial valley is less than 600 m deep over the middle of the segment. Near the segment center the axial valley is so shallow as to be almost unidentifiable (Figure 13b).

ously from ~3050 m to ~3200 m from west to east across the segment (Figure 7) [*Ma and Cochran*, 1997]. This implies either that the strong focusing of melt supply in the center of the segment has occurred extremely recently or that it does not result in a variation in crustal thickness which is preserved onto the ridge flank.

Both the axial depth and gravity are highly asymmetric in segment P3. The shallowest portion of the ridge axis is at about 103°E, only about 10 km from the 102°45'E transform and the depths decrease by less than 100 m from there to the transform (Figure 17). The ridge axis in this area forms a nearly flat plateau. The MBA gravity minimum is located at a small (< 1 km) ridge offset near 103°10'E, about 25 km from the transform (Figures 3 and 17). The change in gravity along the axis from 103°10'E to the 102°45'E transform is 7.5 mGal with a gradient of ~0.3 mGal/km. Axial MBA values increase slowly eastward by about 4 mGal from 103°10'E to 103°32'E in an area where the axis is at a nearly constant depth of slightly over 3000 m within a narrow, shallow valley. East of 103°32'E, the axial depth drops precipitously by ~400 m in a distance of 17 km and then more gradually by another 400 m to reach a depth of 3800 m at the eastern end of the segment as the axis evolves into an 1000 m deep valley. The axial MBA gravity anomalies mirror the axial depth, increasing rapidly by ~10 mGal and then more slowly for a total change of ~21 mGal from the minimum at 103°10'E to the eastern tip of the

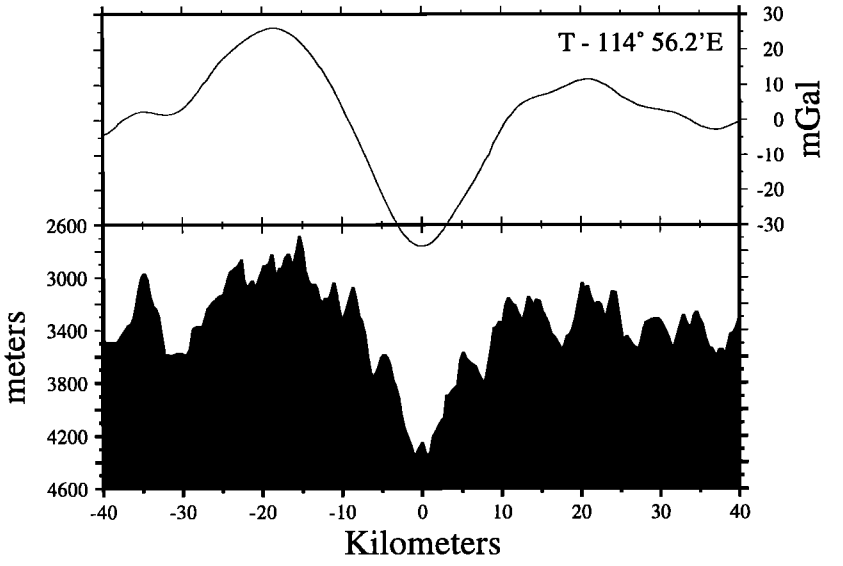

Figure 14. Center beam Seabeam bathymetry and free-air gravity profile across the SEIR axis at 114°56.2'E in segment T, where the axis is characterized by a deep axial valley. The location of the profile is shown in Figure 5. The profile has been projected perpendicular to the axis which is located at 0 km on the horizontal scale. The northern ridge flank is to the right.

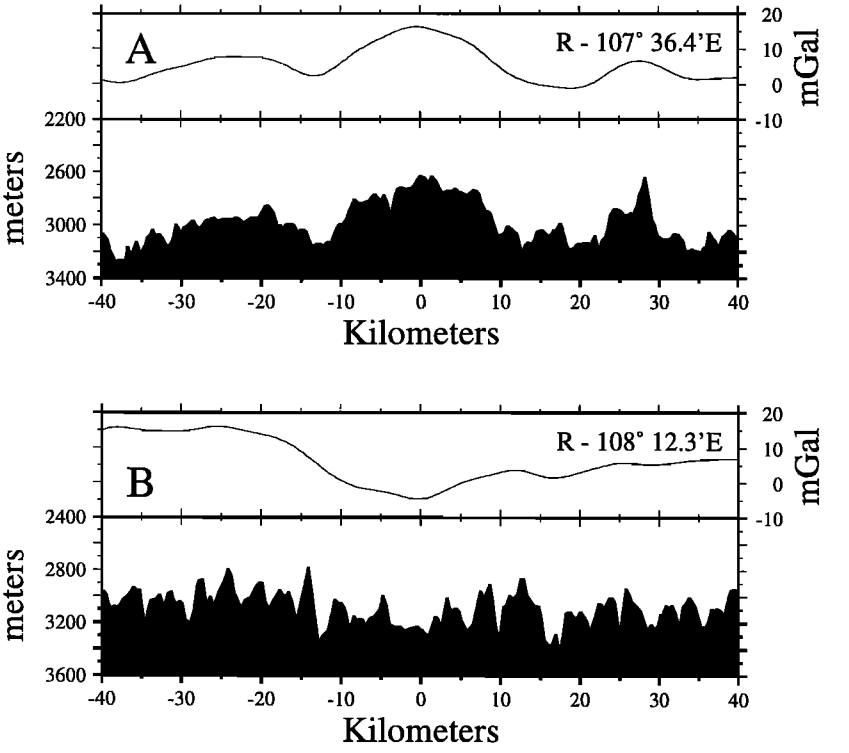

Figure 15. Center beam Seabeam bathymetry and free-air gravity profiles across the SEIR axis from segment R. The location of the profiles is shown in Figure 4. Profiles have been projected perpendicular to the axis which is located at 0 km on the horizontal scale. The ridge axis was located on the basis of an axial magnetic anomaly high. The longitude at which the profiles cross the ridge axis is shown on each profile. The northern ridge flank is to the right. (a) Center of the segment where the axis is marked by a small volcanic ridge atop a broad fault-bounded plateau. (b) Eastern end of the segment where the plateau has died away; the axis is marked by a small valley with a pronounced gravity minimum.

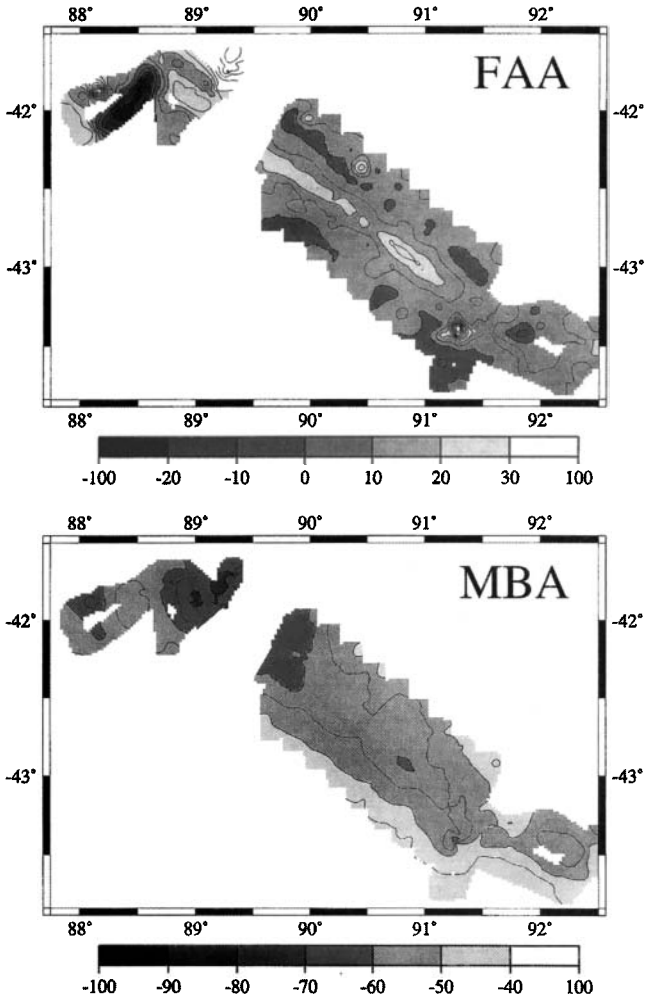

Figure 16a. Free-air anomaly (FAA) and mantle Bouguer anomaly (MBA) gravity maps of survey Box 0 (Figure 2). Contour interval is 5 mGal, and shading changes at 10-mGal intervals. Area from ~89°10'E to ~89°40'E is masked out because the ship tracks were parallel to and a few kilometers from the ridge axis (Figure 2) and thus do not record the full amplitude of the axial anomaly.

segment near 104°18'E (Figure 17). As with segment R, the ridge flank depths do not demonstrate the large variations seen in the axial depth and in the axial MBA profile.

Discussion

Ridge Parallel Changes in Depth

The ~2100 m change in axial depth along the SEIR (Figure 7) consists of two components; a regional change in the depth of the ridge, and a change in the form and amplitude of the axial morphology which is superimposed on the ridge crest. Ma and Cochran [1997] used the empirical orthogonal function (EOF) technique [*Small*, 1994] to decompose the morphology into a "deterministic" component representing the basic shape of the ridge axis and a "stochastic" component representing local tectonic variability. Off-axis ridge-parallel profiles of the deterministic component on both flanks show a regional depth increase of 500 m across the survey area, from ~2800 m in the west near 90°E to ~3300 m in the east near 115°E [*Ma and Cochran*, 1997] (Figure 7). The axial morphology varies from a 200- to 400-m-high axial high west of 103°E (Figures 2, 3 and 10) to a 1200 m-deep valley in segment T [*Sempere et al.*, this issue] (Figures 5 and 14), accounting for the remainder of the 2100 m change in axial depth. The long-wavelength variation in ridge flank depth records the change in mantle temperature and melt supply (crustal thickness), while the variation in the form and amplitude of the axial relief reflects the response of the ridge axis dynamics to these changes in temperature and melt supply.

Gravity Anomalies and Changes in Crustal Thickness and/or Mantle Temperature

The regional variation in both ridge depth and MBA gravity along the SEIR results from a combination of crustal thickness variations and changes in mantle temperature. If the 500-m depth variation is assumed to result only from a change in crustal thickness, simple isostatic considerations put the change in crustal thickness at 1.8-2.4 km depending on the assumed crustal density (in the range of 2700-2900 kg/m^3). If a 2-km decrease in crustal thickness is assumed, it would result in a 50-mGal increase in MBA gravity. This is approximately the change in the level of the MBA gravity along the SEIR from 88°E to 115°E (Figure 7).

The depth change can also be assumed to result from a change in mantle density arising from a west-to east temperature gradient in the mantle with no change in crustal thickness. The magnitude of the density change necessary to create the 500 m difference in ridge depth depends on the depth to which it is assumed to extend. If a compensation depth of 125 km is assumed [*Parsons and Sclater*, 1977], then the required change in the average mantle density is close to 10 kg/m^3. A corresponding temperature difference can be determined as

$$\Delta T = \Delta\rho/\alpha\rho_0 \quad (1)$$

where ρ_0 is a reference mantle density and α is the volumetric coefficient of thermal expansion. This expression predicts a temperature difference of 90°C-100°C depending on the exact choice of α and ρ_0. If the temperature variation is assumed to extend to 200 km [*Klein and Langmuir*, 1987], then the density anomaly is ~6.2 kg/m^3 and the corresponding temperature difference is ~55°C. These two cases predict increases of 49 mGal and 48 mGal, respectively, in MBA gravity between 88°E and 114°E.

These simple calculations varied only crustal thickness or mantle temperature. They thus provide upper bounds on the regional variation in crustal thickness and temperature since, in reality, changes in mantle temperature and crustal thickness (melt supply) are linked and both occur simultaneously across the region. The fact that the long-wavelength variation in MBA gravity is the same for the two end-member calculations means that the gravity data alone cannot distinguish the relative contributions of variations in crustal thickness and mantle temperature. The reason why these different mechanisms predict virtually the same change in MBA gravity is that the same anomalous mass is needed in each case to isostatically support the 500-m depth difference. The assumed variation in crustal and/or mantle structure is very long wavelength and therefore the gravity effect approaches that of an infinite "Bouguer slab" where the gravity effect depends on the anomalous mass but not on distance from the source.

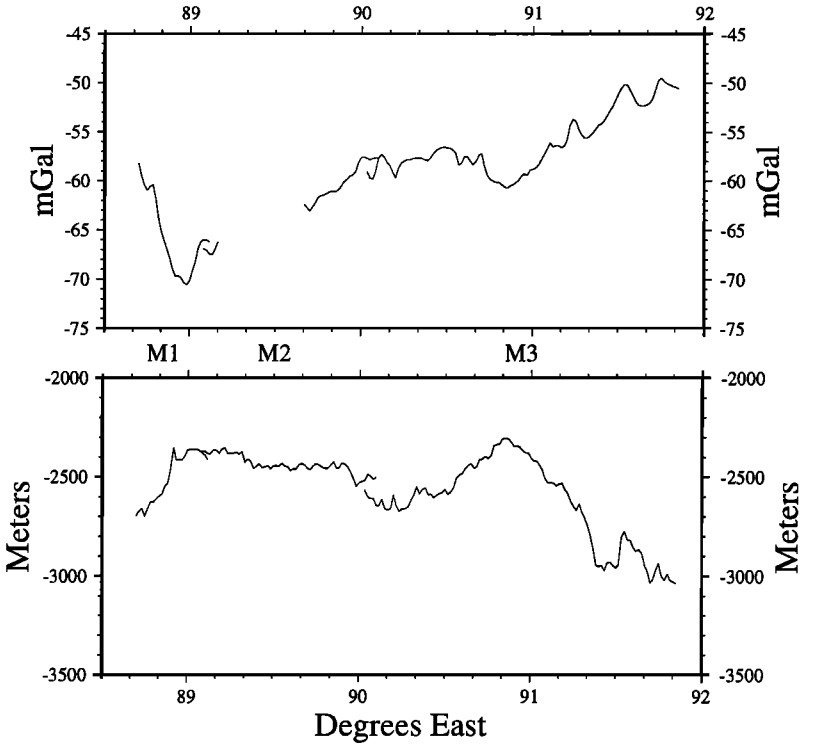

Figure 16b. (bottom) Along-axis depth and (top) along-axis mantle Bouguer anomaly profiles from 88°41'E to 91°51'E (box 0). Segments are identified between the two panels. The region is bounded by a 70-km-offset transform on the west and by a 30-km-offset eastward propagating OSC on the east. The axis between 88°50'E and 89°40'E has an EPR-type axial high. A rifted high is found throughout the remainder of the area (Figure 10b).

Gravity Anomalies and Transitions in Axial Morphology

It is reasonable to assume that the lateral variation in asthenospheric temperature is continuous and smooth. However, the variation in the MBA gravity is not smooth and continuous (Figure 7). Segment scale MBA anomalies are related to the upwelling and melt distribution pattern within individual segments [*Macdonald*, 1989; *Wang and Cochran*, 1993; *Tolstoy et al.*, 1993]. There are also a number of distinct steps in the regional level of the MBA gravity. Although there is a section of the ridge between 92°E and 100°E with insufficient crossings of the axis to confidently determine axial gravity values except at a few locations (Figure 7), the axial MBA values show a fairly uniform regional slope from 89°E to 103.5°E, increasing from -60 mGal to -40 mGal (Figure 7). A 10-mGal step in the gravity occurs from 103.5°E to 104°E within segment P3 (Figures 7 and 17). From 104°E to 114°E, there is again a steady, more gradual slope to the east (albeit with a large intrasegment negative anomaly within segment R). The regional level increases to the east from -30 mGal at 104°E to -20 mGal at 114°E. Another steep regional MBA gradient occurs across and to the east of the 114°E transform. MBA gravity increases from -20 mGal to +5 mGal across segment T (Figures 7 and 19).

The two areas of steep MBA gradients at 103°30'E and 114°E correspond to basic changes in the form of the axial morphology. The MBA gradient at 103°30'E corresponds to the transition from an axial high to a shallow axial valley and the gradient at 114°E corresponds to the transition from a shallow axial valley to a deep MAR-like axial valley. The different forms of axial morphology thus reflect basic changes in the structure of the crust and upper mantle which are significant enough to create a 10-mGal difference in MBA gravity. The step in the MBA level near 103°30'E does not result from a change in crustal thickness, since there is not an accompanying change in ridge flank depths [*Ma and Cochran*, 1997] (Figure 7) as required by isostasy.

The presence of a basic change in ridge axis tectonics accompanying the changes in morphology is also suggested by analysis of the abyssal hills created at segments with differing axial morphology [*Ma et al.*, 1995; *Goff et al.*, 1997; *Ma and Cochran*, 1997]. In particular *Ma and Cochran* [1997] found that bathymetric roughness determined from the stochastic component of their EOF analysis increases by more than a factor of 2 from 88°E to 116°E (Figure 20). However, the increase is not regular but occurs in two discrete steps across the transforms at 102°45'E and 114°E (Figure 20). Segments to the west of 102°45'E with an axial high, whether rifted or EPR-like, form one group. Segments located between 102°45'E and 114°E form a second group. This region includes the transitional segment P3, the "anomalous high" segment R, and segments S1 and S4 characterized by a shallow axial valley. Segment T east of the 114°E transform with a deep axial valley forms a third distinct group. The population of bathymetric roughness estimates at all segments within each region are statistically identical, but they differ significantly between regions with a confidence level of >99% [*Ma and Cochran*, 1997]. Similar results are observed in a covariance analysis of flank morphology [*Goff et al.*, 1997]. The step-like increases

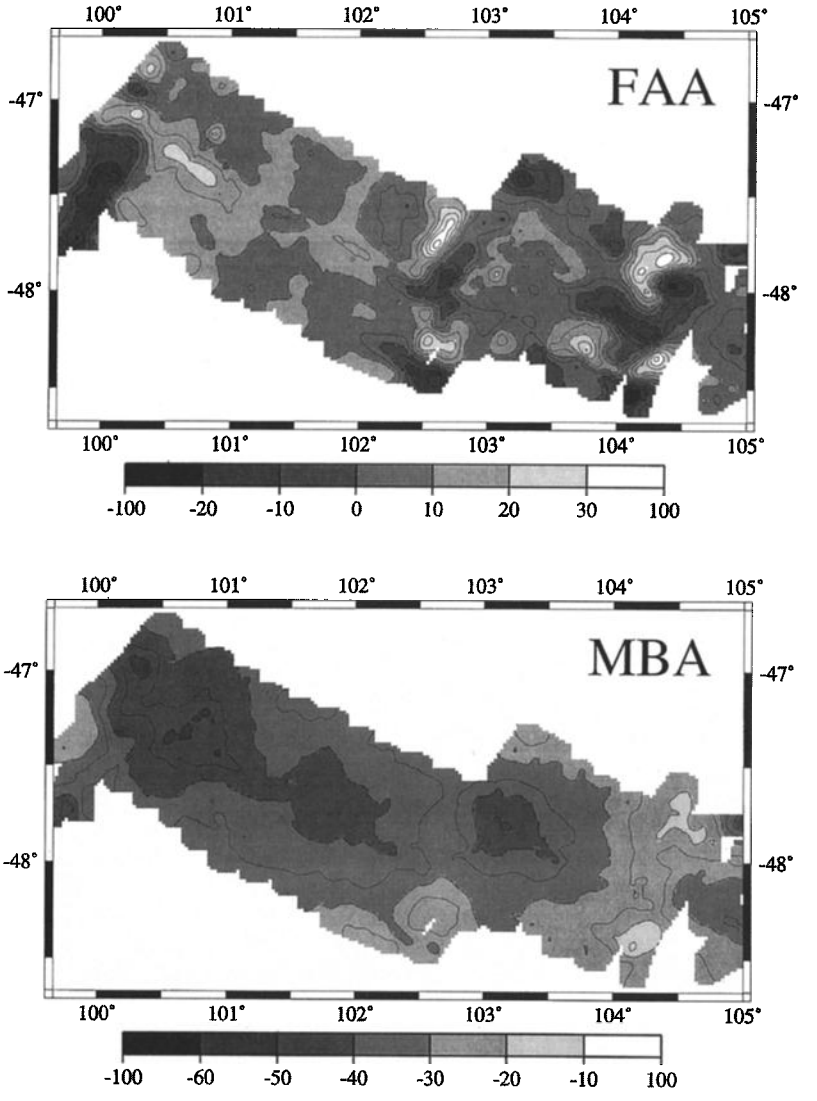

Figure 17a. Free-air anomaly (FAA) and mantle Bouguer anomaly (MBA) gravity maps of survey Box 1 (Figure 3). Contour interval is 5 mGal, and shading changes at 10-mGal intervals.

in bathymetric roughness correspond to the changes observed in the form of the axial morphology and to the steps observed in the level of the MBA gravity.

Model for the Transitions in Morphology

An axial high is considered to result from the upward flexure of weak axial lithosphere by low density asthenosphere beneath the axis [*Madsen et al.*, 1984; *Kuo et al.*, 1986; *Wang and Cochran*, 1993]. The presence of high temperatures and a thin lithospheric lid at axial highs is supported by the common observation of a crustal magma chamber at ridges with an axial high [*Detrick et al.*, 1987; *Mutter et al.*, 1995] and the lack of evidence for a magma chamber at ridges with an axial valley [*Purdy and Detrick*, 1986; *Detrick et al.*, 1990].

The rapid transition from an axial high to an axial valley requires a sudden change in the strength of the lithospheric lid at the axis. *Phipps Morgan and Chen* [1993] have argued that the presence or absence of a crustal magma chamber is itself a threshold phenomenon which has a large effect on the temperature structure and strength of the crust and upper mantle. This occurs largely due to a feedback mechanism in which the latent heat released by freezing of the lower crust within the melt lens tends to encourage formation of an even shallower melt lens. Below some critical melt supply (crustal thickness), a crustal melt lens can not be maintained and this mechanism can not function. *Phipps Morgan and Chen* [1993] calculate that this can lead to a major change in the thermal structure and that the depth to the solidus can increase by several kilometers as the result of a small change in crustal thickness across this threshold.

The transition from an axial high to an axial valley could result from this (or a similar) threshold mechanism. The gradient in asthenospheric temperature along the SEIR and the resulting decrease in melt supply mean that at some point the threshold is reached and a crustal magma lens can not be maintained. The resulting sudden increase in lithospheric strength would suppress the flexure responsible for the axial high and also allow larger faults to form causing the observed step in the bathymetric roughness (Figure 20) and the formation of a shallow valley (Figures 3, 4 and 11). The change in the thermal structure needs to be fairly substantial, however, to account for the observed step in the MBA gravity. If the 10-mGal step in MBA gravity (Figures 7 and 17) is due to an increase in density of a region 5 km thick, then the average

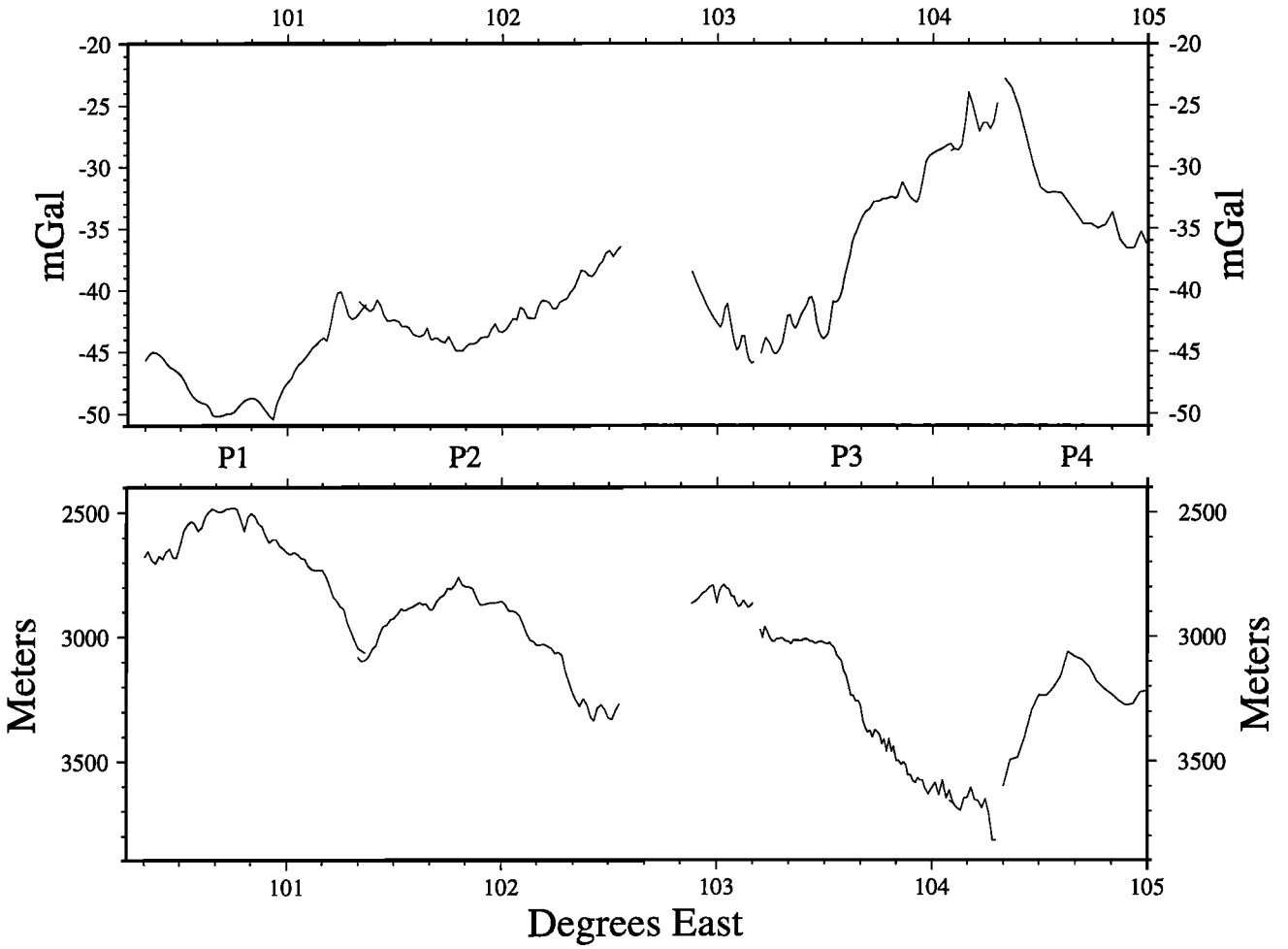

Figure 17b. (bottom) Along-axis depth and (top) along-axis mantle Bouguer anomaly profiles from 100°19'E to 105°E (box 1). Segments are identified between the two panels. The region is bounded on the west by a 130-km offset transform (Figure 3). Segments P1 and P2, west of a 38-km-offset transform near 102°45'E have axial highs (Figures 10a and 10c). Segment P3 from 102°53'E to 104°18'E marks the basic transition from an axial high to the west to an axial valley to the east. Segment P4 east of 104°20'E has a shallow axial valley.

temperature in that region would have to decrease by ~400°K. Note that this large change in shallow temperature structure must result from a very small change in asthenospheric temperature and melt supply.

The transition from "EPR-type" axial high to rifted high appears to be gradational based on their similar ridge flank roughness (Figure 20), gradation in intrasegment form of axial MBA gravity (Figures 16 and 17) and the observation that the EPR-type segments become rifted at segment ends. If a quasi-steady state magma chamber is present at rifted highs, but is deeper and/or attenuated compared to EPR-type highs then the rigid lid will be thicker and stronger reducing the upward flexure of the high and allowing faulting to begin near the axis.

Our observations also suggest that a second sudden transition occurs from a shallow rift valley to a deep rift valley near 114°E. This transition could also result from a threshold effect in which a small change in mantle temperature causes a sudden change in axial tectonics resulting in the formation of a deep rift valley. For example, *Chen and Morgan* [1990] have proposed a mechanism for the creation of a deep axial valley which depends on ability of the ductile lower crust to decouple the rigid lid from shear stresses arising from divergent viscous mantle flow away from the axis. When the ductile region in the lower crust decreases below some critical size the upper crust becomes coupled to the mantle flow resulting in brittle failure and the formation of a deep rift valley

On the other hand, compilations of axial relief [e.g., *Macdonald*, 1986; *Malinverno*, 1993; *Small*, 1994] do not show a sharp break between shallow and deep rift valleys. Rather axial relief appears to increase continuously with decreasing spreading rate. It is thus possible that the sharp break from a shallow axial valley to a deep axial valley at 114°E could be the result of a rapid change in mantle temperature across the western boundary of the AAD similar to that observed across the eastern boundary where there is a very rapid change from an axial high to a deep axial valley across the eastern boundary transform of the AAD at 127°E [*Palmer et al.*, 1993].

Conclusions

1. Axial mantle Bouguer gravity anomalies along the SEIR show a pronounced regional along-axis gradient. Axial MBAs increase from ~-60 mGal near 88°E to ~-10 mGal at 115°E and

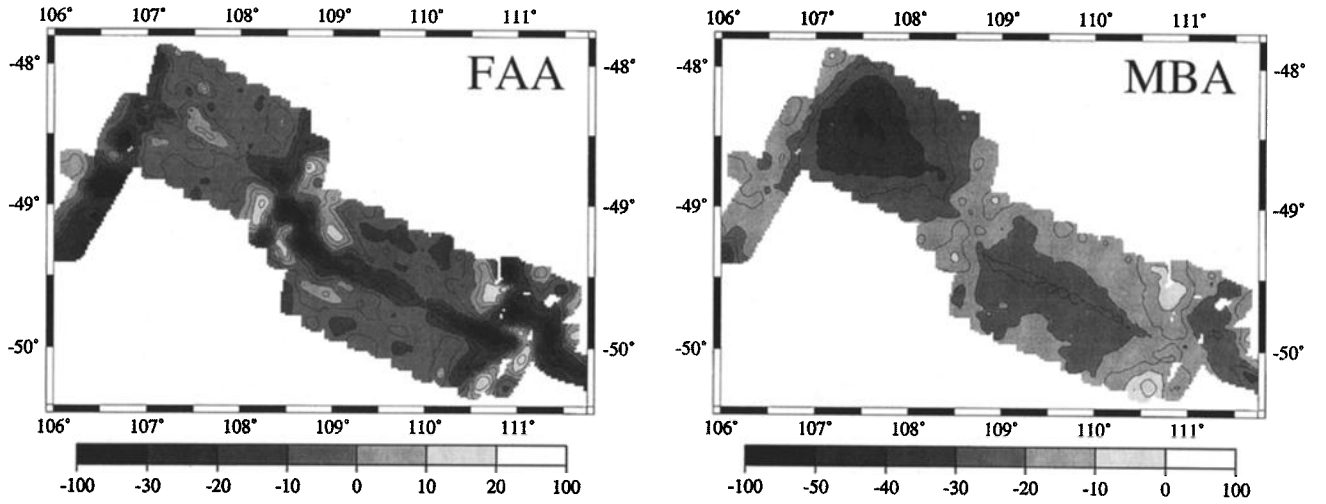

Figure 18a. Free-air anomaly (FAA) and mantle Bouguer anomaly (MBA) gravity maps of survey box 2 (Figure 4). Contour interval is 5 mGal, and shading changes at 10-mGal intervals.

to +5 mGal at the 116°E transform. The MBA gravity gradient is accompanied by a 500 m increase in the depth of the ridge flanks from ~2800 m at 88°E to ~3300 m at 114°E (Figure 7). The regional changes in depth and gravity can both be explained by either a 1.7-2.4 km west to east decrease in crustal thickness or a 55°C-100 °C (depending on the depth to which it extends) west to east decrease in mantle temperature from 88°E to 114°E. In reality, changes in melt supply (crustal thickness) and temperature are linked and will occur simultaneously so that these estimates serve as upper bounds on along-axis changes.

2. The along-axis MBA gravity gradient is not smooth and uniform. Distinct steps in the level of the MBA gravity occurs at two locations, 103°30'E-104°E and 114°E-116°E. The two

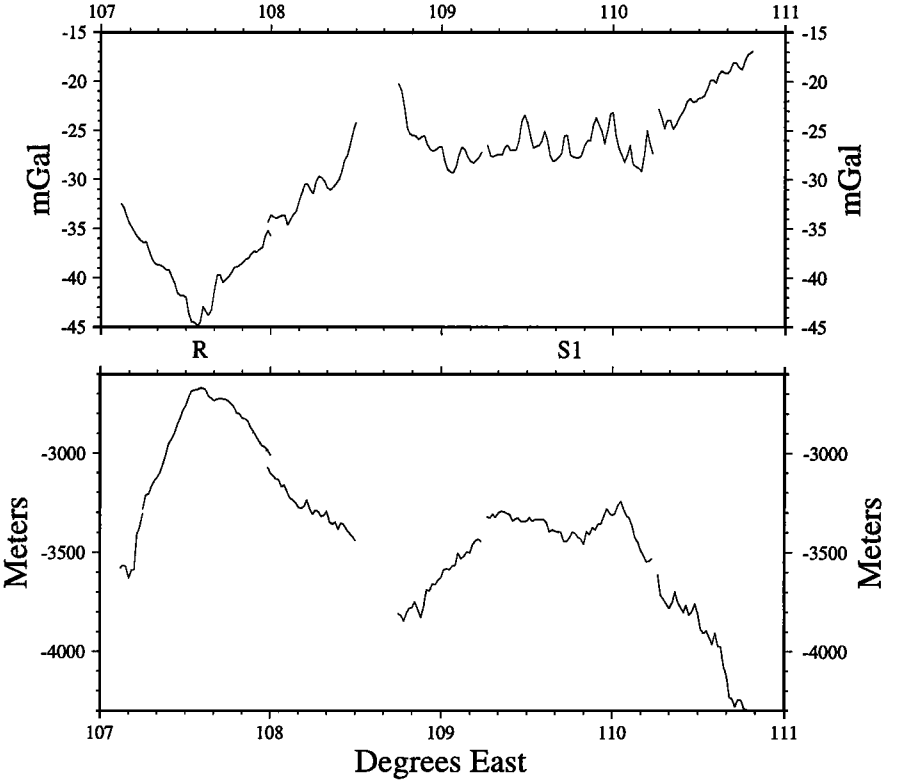

Figure 18b. (bottom) Along-axis depth and (top) along-axis mantle Bouguer anomaly profiles from 107°06'E to 110°49'E (box 2). Segments are identified between the two panels. The ridge axis for the central 50 km of segment R from ~107°20'E to 108°E has a blocky axial high (Figure 15a). The high dies out into an axial valley toward the bounding transforms. Segment S1 has a shallow axial valley which deepens west of 109°15'E toward a complex combination transform-nontransform offset and east of 110°15'E toward a propagating rift tip at 111°E (Figure 13).

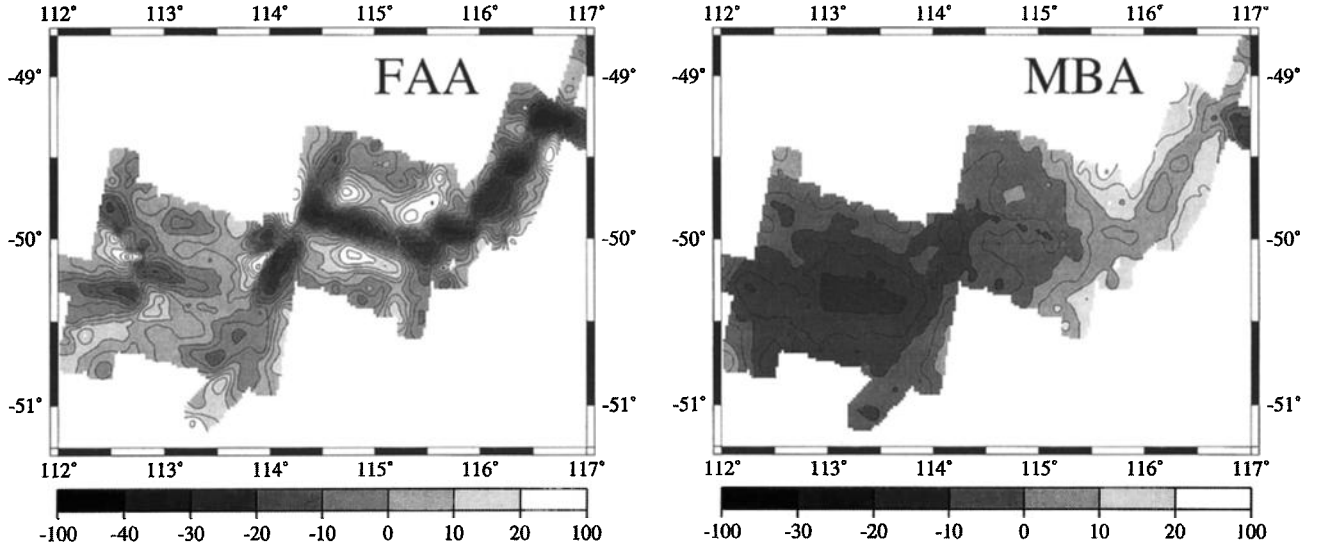

Figure 19a. Free-air anomaly (FAA) and mantle Bouguer anomaly (MBA) gravity maps of survey box 3 (Figure 5). Contour interval is 5 mGal, and shading changes at 10 mGal intervals.

steps in the level of the axial MBA gravity anomalies coincide with sharp steps in ridge flank bathymetric roughness [*Goff et al.*, 1997; *Ma and Cochran*, 1997] (Figure 20) and correspond to fundamental changes in the character of the axial morphology. The ridge axis to the west of 103°E is marked by an axial high. Segments between 104°E and 114°E are generally characterized by shallow axial valleys and the 114°E transform marks the change to a deep MAR-like axial valley. These observations imply that the different types of axial morphology do not simply grade into each other. Rather they represent different forms of axial structure and tectonics with a sharp transition between distinct modes of crustal accretion.

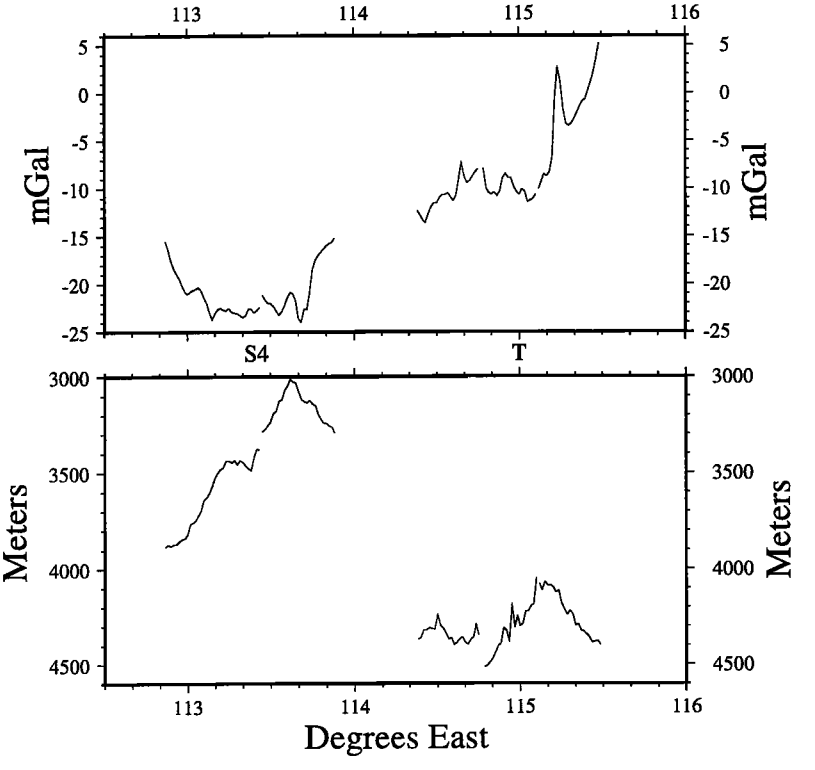

Figure 19b. (bottom) Along-axis depth and (top) along-axis mantle Bouguer anomaly profiles from 112°51'E to 115°29'E (box 3). Segments are identified between the two panels. Segment S4 extends from a retreating rift tip near 112°50'E to a propagating rift tip which has recently collided with the 114°E transform. The axis shallows from steadily from a 1000-m-deep valley at the dying rift tip to a narrow 100-m-high volcanic ridge near 113°50'E before deepening slightly into a shallow valley at its eastern end. Segment T is characterized by a deep (~1200 m) axial valley for its entire length.

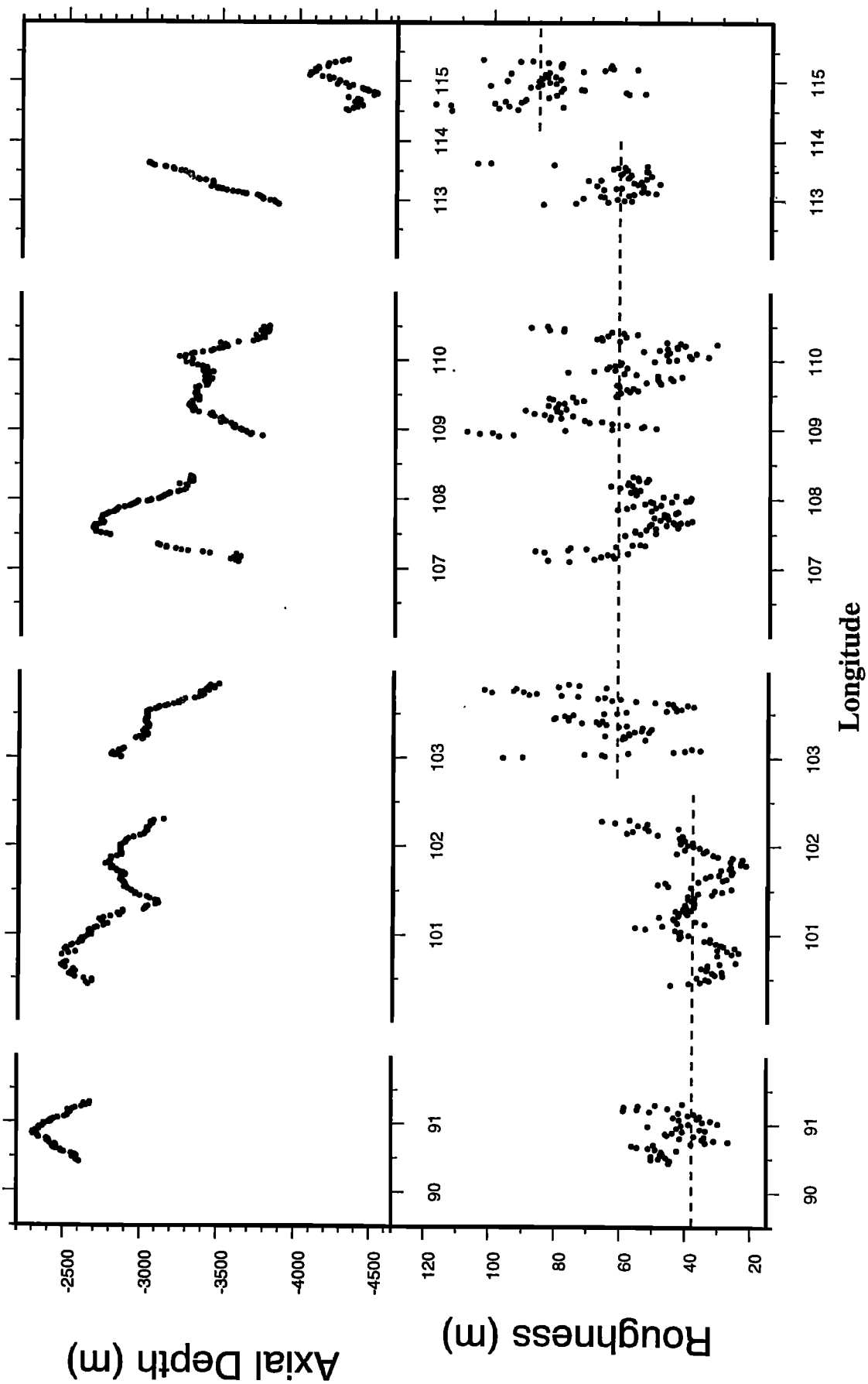

Figure 20. top) Axial depth and (bottom) ridge flank bathymetric roughness for the eight segments within the detailed study boxes. Bathymetric roughness was determined by *Ma and Cochran* [1997] using the empirical orthogonal function technique, and is defined as the median absolute deviation of the "stochastic" or local component of the bathymetry [*Small*, 1994]. Note the step-like increases in bathymetric roughness near 103°E and 114°E that correspond to the changes from an axial high to a shallow axial valley and from a shallow to a deep axial valley.

The transition from an axial high to a shallow valley requires a rapid increase in the strength (thickness) of the lithospheric lid, both to suppress the upward flexure responsible for the axial high [*Madsen et al.*, 1984; *Kuo et al.*, 1986; *Wang and Cochran*, 1993] and to allow the formation of larger throw faults. A threshold mechanism such as that proposed by *Phipps Morgan and Chen* [1993] is necessary to explain the rapid, coincident changes in axial morphology, ridge flank roughness and axial MBA gravity. *Phipps Morgan and Chen* [1993] argue that there is a critical melt supply (crustal thickness) below which a crustal melt lens cannot be maintained and that the depth to the solidus can increase by several kilometers as the result of a small decrease in crustal thickness across this threshold. This change in thermal structure could result in the necessary increase in axial lithospheric strength. The change in thermal structure must be significant to account for the 10-mGal step in the MBA gravity. If the change in gravity results from higher densities in the upper 5 km of the mantle, then the average temperature in that region must decrease by 400°K.

The transition from a shallow axial valley to a deep axial valley at 114°E could result from a second threshold phenomenon, such as that proposed by *Chen and Morgan* [1990]. However, it might also result from a very rapid change in mantle temperature at the western boundary of the AAD, similar to the change observed at the eastern boundary [*Klein et al.*, 1991; *Sempere et al.*, 1991; *Palmer et al.*, 1993].

3. The different forms of axial morphology along the SEIR are associated with different intrasegment MBA gravity patterns. Segments with an axial high have MBA lows located at a depth minimum near the center of the segment. Surveyed segments with an EPR-like axial high have bull's eye MBA anomalies with 10-15 mGal lows and along-axis gradients of 0.15-0.25 mGal/km, similar to what is observed at the EPR [*Wang and Cochran*, 1993]. Segments with a rifted axial high have shallower gravity minima and lower gradients. The gravity anomalies at rifted highs as well as the presence of pervasive faulting across these axial highs can be explained as the result of a deeper or attenuated melt lens and composite magma chamber [*Sinton and Detrick*, 1992] in the lower crust and upper mantle as a the result of a reduced and perhaps episodic melt supply.

Segments with a shallow axial valley are characterized by a lack of correspondence between axial depth and axial MBA values and have a very flat (<3 mGal variation) along-axis MBA profile away from segment bounding ridge offsets. The exception to this pattern is segment R where the axis along the central 50 km of the segment is a volcanic ridge at the summit of a 20 km wide fault-bounded plateau. This segment is characterized by very large along-axis changes in axial depth (950 m) and in MBA gravity (20 mGal) with an MBA gradient of 0.35 mGal/km. Both of these characteristics indicate very vigorous upwelling of melt beneath the segment. However, this segment has ridge flank abyssal hill amplitudes characteristic of segments with a shallow axial valley [*Goff et al.*, 1997; *Ma and Cochran*, 1997] (Figures 7 and 20). It may represent the interaction of a ridge axis having a temperature structure which would normally produce a shallow axial valley with a melt anomaly.

Only one segment with a deep MAR-like rift valley was included in the survey area (segment T, near 115°E at the eastern end of the survey region). Segment T does not however have along-axis depth and gravity profiles characteristic of segments on the MAR. An 80 km-long segment such as segment T would be expected to have ~1400 m of along-axis depth relief associated with a 30 mGal MBA gravity low, according to relationships developed at the MAR [*Lin et al.*, 1990; *Detrick et al.*, 1995]. Instead, it has only ~450 m of along-axis depth relief and no real intrasegment MBA minimum (Figure 19). However, this segment is located in a region with a very steep regional MBA gradient (Figures 7 and 19) and probably marks the effective western boundary of the AAD. The depth and gravity pattern at the segment may be perturbed by a rapid change in asthenospheric temperature across the boundary of the AAD. We have insufficient data to determine whether segments farther to the east within the AAD have a gravity pattern more characteristic of the MAR.

Acknowledgments. We thank Captain E. Buck and the crew of the R/V *Melville* for their assistance during the field program which led to the collection of high quality data during often difficult weather and sea conditions. We also thank S. Smith, U. Albright, T. Porteus, E. Heckman and J. Skinner of Scripps Institution of Oceanography for technical help during cruises WEST09MV and WEST10MV. The GMT [*Wessel and Smith*, 1995] and MBsystem (D. Chayes and D. Caress, pers. comm.) software packages were extensively used in the preparation of this paper. Careful reviews of the manuscript by Jill Karsten, Greg Neumann and Paul Wessel were extremely helpful. This work was funded by National Science Foundation grants OCE-93-02091 (JRC) and OCE-94-03583 (JCS). Lamont-Doherty contribution number 5638.

References

Bell, R. E., and A. B. Watts, Evaluation of the BGM-3 sea gravity meter system onboard R/V *Conrad*, *Geophysics, 51,* 1480-1493, 1986.

Cande, S. C., and J. C. Mutter, A revised identification of the oldest seafloor spreading anomaly between Australia and Antarctica, *Earth Planet. Sci. Lett., 58,* 151-161, 1982.

Chen, Y. J., and W. J. Morgan, Rift valley/no rift valley transition at mid-ocean ridges, *J. Geophys. Res., 95,* 17,571-17,581, 1990.

Cochran, J. R., Systematic variation of axial morphology along the Southeast Indian Ridge (abstract), *Eos Trans. AGU, 72,* 260, 1991.

DeMets, C., R. G. Gordon, D. F. Argus, and S. Stein, Current plate motions, *Geophys. J. Int., 101,* 425-478, 1990.

Detrick, R. S., P. Buhl, E. E. Vera, J. C. Mutter, J. A. Orcutt, J. A. Madsen, and T. M. Brocher, Multichannel seismic imaging of the axial magma chamber along the East Pacific Rise between 9°N and 13°N, *Nature, 326,* 35-41, 1987.

Detrick, R. S., J. C. Mutter, P. Buhl, and I. I. Kim, No evidence from multichannel reflection data for a crustal magma chamber in the MARK area on the Mid-Atlantic Ridge, *Nature, 347,* 61-64, 1990.

Detrick, R. S., H. D. Needham, and V. Renard, Gravity anomalies and crustal thickness variations along the Mid-Atlantic Ridge between 33°N and 40°N, *J. Geophys. Res., 100,* 3767-3787, 1995.

Forsyth, D. W., R. L. Ehrenbard, and S. Chapin, Anomalous upper mantle beneath the Australian-Antarctic Discordance, *Earth Planet. Sci. Lett., 84,* 471-478, 1987.

Goff, J. A., Y. Ma, A. Shah, J. R. Cochran, and J.-C. Sempere, Stochastic analysis of seafloor morphology on the flanks of the Southeast Indian Ridge: The influence of ridge morphology on the formation of abyssal hills, *J. Geophys. Res., in press,* 1997.

Heezen, B. C., The rift in the ocean floor, Sci. Am., *203,* 99-110, 1960.

Johnson, K. T. M., D. S. Scheirer, D. W. Forsyth, and D. W. Graham, *Cruise report: Boomerang expedition, Leg 06, R/V Melville*, 48 pp., Bishop Mus., Honolulu, Hawaii, 1996.

Klein, E. M., and C. H. Langmuir, Global correlations of ocean ridge basalt chemistry with axial depth and crustal thickness, *J. Geophys. Res., 92,* 8089-8115, 1987.

Klein, E. M., C. H. Langmuir, and H. Staudigel, Geochemistry of basalts from the southeast Indian Ridge, 115°E-138°E, *J. Geophys. Res., 96,* 2089-2108, 1991.

Kuo, B. Y., D. Forsyth, and E. M. Parmentier, Flexure and thickening of the lithosphere at the East Pacific Rise, *Geophys. Res. Lett., 13,* 681-684, 1986.

Lin, J., and J. Phipps Morgan, The spreading rate dependence of three-dimensional mid-ocean ridge gravity structure, *Geophys. Res. Lett., 19,* 13-16, 1992.

Lin, J., G. M. Purdy, H. Shouten, J. C. Sempere, and C. Zervas, Evidence from gravity data for focused magmatic accretion along the Mid-Atlantic Ridge, *Nature, 344,* 627-632, 1990.

Ma, Y., and J. R. Cochran, Transitions in axial morphology along the Southeast Indian Ridge, *J. Geophys. Res., 101,* 15,849-15,866, 1996.

Ma, Y., and J. R. Cochran, Bathymetric roughness of the Southeast Indian Ridge: Implications for crustal accretion at intermediate spreading rate mid-ocean ridges, *J. Geophys. Res., in press,* 1997.

Ma, Y., J. R. Cochran, C. Small, and J.-C. Sempere, The Southeast Indian ridge between 88°E and 120°E: Ridge flank morphology and abyssal hills (abstract), *Eos Trans. AGU, 76,* F529, 1995.

Macdonald, K. C., The crest of the Mid-Atlantic Ridge: Models for crustal generation processes and tectonics, in *The Geology of North America*, vol. M, *The Western North Atlantic Region*, edited by P. Vogt and B. Tucholke, pp. 51-68, Geol. Soc. of Am., Boulder, Colo., 1986.

Macdonald, K. C., Tectonic and magmatic processes on the East Pacific Rise, in *The Geology of North America*, vol. N, *The Eastern Pacific Ocean and Hawaii*, edited by E. L. Winterer, D. M. Hussong and R. W. Decker, pp. 93-110, Geol. Soc. of Am., Boulder, Colo., 1989.

Macdonald, K. C., P. J. Fox, L. J. Perram, M. F. Eisen, R. M. Haymon, S. P. Miller, S. M. Carbotte, M. H. Cormier, and A. N. Shor, A new view of the mid-ocean ridge from the behaviour of ridge-axis discontinuities, *Nature, 335,* 217-225, 1988.

Macdonald, K. C., D. S. Scheirer, and S. M. Carbotte, Mid-ocean ridges: Discontinuities, segments and giant cracks, *Science, 253,* 986-994, 1991.

Madsen, J. A., D. W. Forsyth, and R. S. Detrick, A new isostatic model for the East Pacific Rise crest, *J. Geophys. Res., 89,* 9997-10,016, 1984.

Malinverno, A., Transition between a valley and a high at the axis of the mid-ocean ridges, *Geology, 21,* 639-642, 1993.

Menard, H. W., The East Pacific Rise, *Science, 132,* 1737-1746, 1960.

Mutter, J. C., S. M. Carbotte, W. Su, L. Xu, P. Buhl, R. S. Detrick, G. A. Kent, J. A. Orcutt, and A. J. Harding, Seismic images of active magma systems beneath the East Pacific Rise between 17°05' and 17°35'S, *Science, 268,* 391-395, 1995.

Palmer, J., J. C. Sempere, D. M. Christie, and J. Phipps Morgan, Morphology and tectonics of the Australian-Antarctic Discordance between 123°E and 128°E, *Mar. Geophys. Res., 15,* 121-152, 1993.

Parker, R. L., The rapid calculation of potential anomalies, *Geophys. J. R. Astron. Soc., 31,* 447-455, 1973.

Parsons, B., and J. G. Sclater, Ocean floor bathymetry and heat flow, *J. Geophys. Res., 82,* 803-827, 1977.

Phipps Morgan, J., and Y. J. Chen, Dependence of ridge-axis morphology on magma supply and spreading rate, *Nature, 364,* 706-708, 1993.

Phipps Morgan, J., E. M. Parmentier, and J. Lin, Mechanisms for the origin of mid-ocean ridge axial topography: Implications for the thermal and mechanical structure of accreting plate boundaries, *J. Geophys. Res., 92,* 12,823-12,836, 1987.

Prince, R. A., and D. W. Forsyth, Horizontal extent of anomalously thin crust near the Vema Fracture Zone from the three-dimensional analysis of gravity anomalies, *J. Geophys. Res., 93,* 8051-8063, 1988.

Purdy, G. M., and R. S. Detrick, Crustal structure of the Mid-Atlantic Ridge at 23°N from seismic refraction, *J. Geophys. Res., 91,* 3739-3762, 1986.

Pyle, D. G., *Geochemistry of mid-ocean ridge basalt within and surrounding the Australian-Antarctic Discordance*, Ph.D., Oregon State University, 178 pp., 1994.

Royer, J.-Y., and D. T. Sandwell, Evolution of the eastern Indian Ocean since the late Cretaceous: Constraints from Geosat altimetry, *J. Geophys. Res., 94,* 13,755-13,782, 1989.

Royer, J. Y., and R. Schlich, Southeast Indian Ridge between the Rodriquez triple junction and the Amsterdam and Saint Paul Islands: Detailed kinematics for the past 20 m.y., *J. Geophys. Res., 93,* 13,524-13,550, 1988.

Sempere, J. C., G. M. Purdy, and H. Schouten, Segmentation of the Mid-Atlantic Ridge between 24°N and 30°40'N, *Nature, 344,* 427-431, 1990.

Sempere, J. C., J. Palmer, D. M. Christie, J. Phipps Morgan, and A. N. Shor, Australian-Antarctic discordance, *Geology, 19,* 429-432, 1991.

Sempere, J. C., J. Lin, H. S. Brown, H. Schouten, and G. M. Purdy, Segmentation and morphologic variations along a slow-spreading center: The Mid-Atlantic Ridge (24°00'N-30°40'N), *Mar. Geophys. Res., 15,* 153-200, 1993.

Sempere, J. C., J. R. Cochran, and the SEIR Scientific Team, The Southeast Indian Ridge between 88°E and 120°E: Variations in crustal accretion at constant spreading rate, *J. Geophys. Res, this issue,* 1997.

Sinton, J. M., and R. S. Detrick, Mid-ocean ridge magma chambers, *J. Geophys. Res., 97,* 197-216, 1992.

Small, C., A global analysis of mid-ocean ridge axial topography, *Geophys. J. Int., 116,* 64-84, 1994.

Small, C., and D. T. Sandwell, An abrupt change in ridge axis gravity with spreading rate, *J. Geophys. Res., 94,* 17,383-17,392, 1989.

Small, C., and D. T. Sandwell, An analysis of ridge axis gravity roughness and spreading rate, *J. Geophys. Res., 97,* 3235-3245, 1992.

Small, C., and D. T. Sandwell, Imaging mid-ocean ridge transitions with satellite gravity, *Geology, 22,* 123-126, 1994.

Smith, W. H. F., and P. Wessel, Gridding with continuous curvature splines in tension, *Geophysics, 55,* 293-305, 1990.

Tolstoy, M., A. J. Harding, and J. A. Orcutt, Crustal thickness on the Mid-Atlantic Ridge: Bull's eye gravity anomalies and focused accretion, *Science, 262,* 726-729, 1993.

Tolstoy, M., A. J. Harding, J. A. Orcutt, and J. Phipps Morgan, Crustal thickness at the Australian Antarctic

Discordance and neighboring Southeast Indian Ridge, *Eos Trans. AGU, 76(46),* F570, 1995.

Tucholke, B. E., and J. Lin, A geologic model for the structure of ridge segments in slow spreading ocean crust, *J. Geophys. Res., 99,* 11,937-11,958, 1994.

Veevers, J. J., Breakup of Australia and Antarctica estimated as mid-Cretaceous (95±5 Ma) from magnetic and seismic data at the continental margin, *Earth Planet. Sci. Lett., 77,* 91-99, 1986.

Wang, X., and J. R. Cochran, Gravity anomalies, isostasy and mantle flow at the East Pacific Rise crest, *J. Geophys. Res., 98,* 19,505-19,531, 1993.

Wang, X., and J. R. Cochran, Along-axis gravity gradients at mid-ocean ridges: Implications for mantle flow and axis morphology, *Geology, 23,* 29-32, 1995.

Wessel, P., and W. H. F. Smith, A new version of the Generic Mapping Tools (GMT), *Eos Trans. AGU, 76,* 329, 1995.

West, B. P., J.-C. Sempere, D. G. Pyle, J. Phipps Morgan, and D. M. Christie, Evidence for variable upper mantle temperature and crustal thickness in and near the Australian-Antarctic Discordance, *Earth Planet. Sci. Lett., 128,* 135-153, 1994.

D. Christie and B. Sylvander, College of Oceanic and Atmospheric Sciences, Oregon State University, Corvallis, OR 97331-5503

J. R. Cochran, Y. Ma, C. Small, and W. Zhang, Lamont-Doherty Earth Observatory of Columbia University, Palisades, NY 10964

M. Eberle, Department of Geological Science, Brown University, Providence, RI 02912

L. Gelí, Départment de Géosciences Marines, IFREMER, B.P. 70, 29280, Plouzané, France

J. A. Goff, University of Texas Institute of Geophysics, 8701 MoPac Expressway,Austin, TX 78759

H. Kimura, Earthquake Research Institute, University of Tokyo, 1-1-1 Yayoi, Bunkto-ku, Tokyo 113, Japan

J.-C. Sempéré, Exxon Production Research Company, P.O. Box 2189, Houston, TX 77252-2189

A. Shah and B.P. West, School of Oceanography, University of Washington, Seattle, WA 98195-7940

(Received August 23, 1996; revised January 20, 1997;
accepted February 13, 1997.)